

1 **Evaluating modelling decisions and spatial predictions in**
2 **ecosystem mapping**

3 **Authors:**

4 Alys R. Young^{1,2}, Nicholas J. Murray³, Jane Elith², Brett A. Bryan¹, Hugh F. Davies^{4,5}, and
5 Emily Nicholson²

6 **Affiliations:**

7 ¹ School of Life and Environmental Sciences, Faculty of Science, Engineering, and Built
8 Environment, Deakin University, Burwood VIC 3125 Australia

9
10 ² School of Agriculture, Food and Ecosystem Science, Faculty of Science, The University of
11 Melbourne, Parkville VIC 3010 Australia

12
13 ³ College of Science and Engineering, James Cook University, Townsville QLD 4811
14 Australia

15
16 ⁴ Research Institute for the Environment and Livelihoods, Charles Darwin University,
17 Casuarina NT 0909 Australia

18
19 ⁵ Centre for Ecosystem Science, School of Biological, Earth and Environmental Science,
20 University of New South Wales, Sydney NSW 1466 Australia

21 **Corresponding author:**

22 Alys Young

23 a.young@research.deakin.edu.au

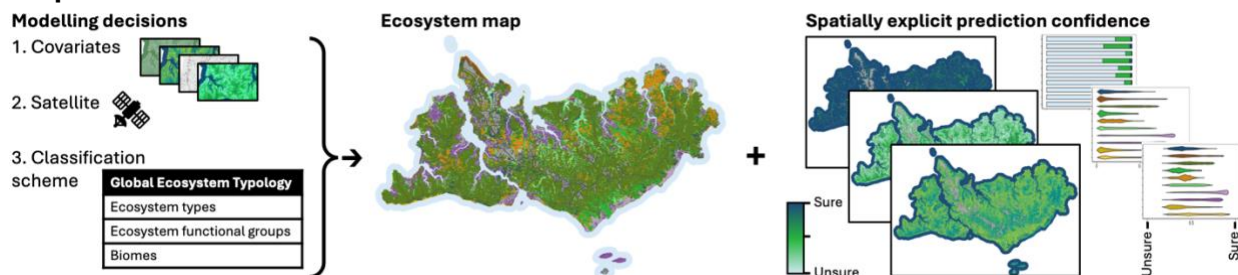
24 alysy.research@gmail.com

25 ORCID 0000-0002-9562-2253

26 **Abstract**

27 Ecosystem maps support a vast array of applications in conservation, land management
28 and policy. The capacity of an ecosystem map to support these applications is determined
29 by its ability to accurately represent ecosystem distributions, which is heavily influenced
30 by the model used to produce them. Here, we evaluated the influence of key modelling
31 decisions made whilst developing a new and comprehensive ecosystem map using a
32 recently developed ecosystem typology for the remote Tiwi Islands, Australia. We collated
33 a reference set of training points from diverse datasets and employed a pixel-based,
34 random forest model to classify and predict ecosystem distributions. We tested decisions
35 at three stages of the model formulation. First, we tested the number of classes by
36 aggregating ecosystem types (finest scale, n = 11) into functional groups (n = 10) and
37 biomes (coarsest, n = 8) according to the Global Ecosystem Typology. Second, we
38 compared data acquired from the Sentinel-2 satellite using the MSI sensor and Landsat-9
39 with the OLI-2 sensor. Finally, we tested covariates from satellite image bands only or
40 satellite imagery combined with additional covariates describing other ecological
41 characteristics. We evaluated these decisions using a range of model performance
42 metrics, including overall, by-class and spatially explicit estimates. Our study found that
43 using covariates additional to those from satellite images improved all evaluation metrics
44 for all model decisions. Acquisitions from Landsat-9 tended to improve model
45 performance over Sentinel-2, although the effect was variable. Developing maps at the
46 biome scale (coarsest resolution) slightly improved overall performance but hinders
47 applications that need to differentiate between ecosystem types. Including additional
48 relevant covariates or considering alternative satellites are better options for improving
49 map performance than simplifying the classes. Producing spatially explicit evaluation of
50 ecosystem maps is a rapid and achievable method to communicate limitations and
51 support users to make informed decisions.

52 **Graphical abstract**



53

54 **Key words:**

55 Remote sensing, Earth observation, vegetation mapping, land cover, island ecology,
56 tropical savanna, machine learning, biogeography

57 **1. Introduction**

58 Ecosystem distribution maps form a crucial foundation to understand, monitor, and make
59 decisions about the environment. Applications of ecosystem maps span conservation
60 assessments (Murray *et al.*, 2017; Keith, Ferrer-Paris, *et al.*, 2024), spatial planning
61 (Watson *et al.*, 2023; Keith, Ghoraba, *et al.*, 2024), valuing services (Hein *et al.*, 2020; Xiao
62 *et al.*, 2024) and reporting (Watson *et al.*, 2020; Nicholson *et al.*, 2024). The usefulness of
63 an ecosystem map in these contexts is determined by its ability to accurately model and
64 represent the distributions of ecosystem classes in geographic space.

65
66 As ecosystem maps are models of the natural world, decisions made during the modelling
67 process can strongly impact outcomes (Gould *et al.*, 2023). Variations due to modelling
68 decisions, model uncertainty, and errors (henceforth, ‘map reliability’) propagate through
69 to applications (Burgman, Lindenmayer and Elith, 2005; Jansen *et al.*, 2022), and influence
70 area estimates (Olofsson *et al.*, 2020; Naas *et al.*, 2023), ecosystem accounting (Venter *et al.*
71 *et al.*, 2024), and assessments (De la Cruz *et al.*, 2017). Therefore, it is important to assess
72 the main decisions influencing reliability and communicate the remaining error and
73 uncertainty to users.

74
75 Evaluating modelling decisions is common in other spatial modelling applications,
76 including for landcover which typically focus on structural elements of the landscape,
77 land-use mapping, and species distribution models (Khatami, Mountrakis and Stehman,
78 2016; Grimmett, Whitsed and Horta, 2020). Fewer studies have examined the impacts of
79 model formulation in ecosystem mapping which presents a unique and challenging case
80 study (Rocchini *et al.*, 2013). Ecosystems are defined by a unique biotic community, the
81 abiotic environment, and driving ecological processes (CBD, 1992). Thus, ecosystem
82 classes can be difficult to visibly distinguish using remotely sensed data. For instance,
83 forest ecosystem types delineated by distinct understories but displaying similar canopy
84 composition and physical structure are indistinguishable with multispectral imagery
85 (Trouvé *et al.*, 2023). Ecosystems also exhibit complex spatiotemporal dynamics because
86 of ecological processes, natural variation, and disturbance (Dryflor *et al.*, 2016; Dorrough
87 *et al.*, 2021; Keith *et al.*, 2022). Finally, the number of ecosystem types are typically higher
88 than in landcover classification. For instance, 98 ecosystem types are described for Italy
89 compared to 66 landcover classes (Capotorti *et al.*, 2023).

90
91 Key factors of model formulation known to influence ecosystem maps include the
92 comprehensiveness of the typology (Foody, 2021), the reference data and classification of
93 location into the ecosystem classes (Rocchini *et al.*, 2013; Dorrough *et al.*, 2021; Naas *et al.*
94 *et al.*, 2023), covariates (Simensen *et al.*, 2020; Trouvé *et al.*, 2023; Naas *et al.*, 2024), and
95 output post-processing (Horvath *et al.*, 2021). Since ecosystem mapping stems from a
96 long history of landcover mapping, the effects of some decisions can be inferred, such as
97 the benefit of covariates, the challenge of many classes, and model types (Yu *et al.*, 2014;
98 Khatami, Mountrakis and Stehman, 2016). Understanding the key factors and the
99 interaction of these factors specific to ecosystems would provide crucial guidance for
100 ecosystem map development, especially important given the given growing focus on

101 developing ecosystem maps at global, national, and regional scales (Galaz García *et al.*,
102 2023).

103
104 In addition to understanding sources of uncertainty in the model formulation, there is a
105 long and growing interest in spatially explicit evaluation metrics to communicate map
106 reliability. Such approaches have emerged in response to current limitations of evaluation
107 assessments (Stehman and Foody, 2019; Foody, 2021) and as a result of modelling
108 advances (Loosvelt *et al.*, 2012; Mitchell, Downie and Diesing, 2018). Spatially explicit
109 evaluation metrics complement confusion matrix-based evaluation by emphasising spatial
110 patterns and facilitate uncertainty propagation into downstream products (Foody, 2002;
111 Jansen *et al.*, 2022). Here, we refer to these spatially explicit evaluation metrics as
112 ‘prediction confidence’ due to their focus on the probability of class membership (McIver
113 and Friedl, 2001; Mitchell, Downie and Diesing, 2018), and acknowledge that high
114 confidence is not synonymous with high accuracy (Stehman and Foody, 2019). Spatially
115 explicit metrics are yet to become standard practice and require further demonstrations in
116 new applications.

117
118 In this paper, we sought to evaluate the effects of modelling decisions on ecosystem
119 maps, using the case study of the Tiwi Islands, Australia. On the Indigenous-owned and
120 managed Tiwi Islands, ecosystem maps inform development decisions and management
121 actions (e.g. Richards *et al.*, 2012). We tested the sensitivity of the map reliability to three
122 modelling decisions. Firstly, to represent decisions related to the classification scheme,
123 we used a hierarchical ecosystem typology (Young *et al.*, 2024) that is aligned with the
124 Global Ecosystem Typology (GET, global-ecosystems.org), an internationally accepted
125 classification of ecosystems (UNSD, 2021; Keith *et al.*, 2022). Different levels of a
126 classification hierarchy are ideal for systematically testing the number of classes which
127 change in relation to the thematic resolution (also called thematic scale or class
128 resolution). Secondly, to examine the impact of the choice of satellite, we compared
129 model covariates retrieved from the Landsat-9 satellite with the Operational Land Imager
130 (OLI-2) sensor against the Sentinel-2 satellite with the Multispectral imager (MSI) sensor.
131 The Landsat and Sentinel missions represent two flagship programs providing open-
132 access satellite images (Wulder *et al.*, 2012) and vary in spatial and spectral resolution,
133 length of time series and processing. Thirdly, to assess the implications of model
134 covariates on map reliability, we investigated the use of only satellite image covariates and
135 compared these to models that also include other ecologically meaningful covariates
136 (hereafter named “additional” covariates). Covariates such as elevation and those
137 representing vegetation structure (e.g. canopy height) often improve ecosystems and
138 landcover models (Khatami, Mountrakis and Stehman, 2016; Simensen *et al.*, 2020; Trouvé
139 *et al.*, 2023). We demonstrate three spatially explicit maps of prediction confidences to
140 accompany the ecosystem map which can inform managers of map reliability and improve
141 conservation outcomes.

142 **2. Materials and methods**

143 **2.1 Case study location**

144 The Tiwi Islands, including Melville Island (5,788 km²), Bathurst Island (1,693 km²) and
145 numerous small islands, are located off the northern coast of the Northern Territory,
146 Australia. The Tiwi Islands are in the Australian “Tiwi-Coburg” bioregion (DCCEEW, 2021)
147 and the global “Arnhem Land tropical savanna” ecoregion (Olson *et al.*, 2001). The lands
148 and waters of the Tiwi Islands are managed by the Indigenous Tiwi peoples. Much of the
149 Islands are remote and challenging to access (Figure 1).

150 **2.2 Classification scheme**

151 To investigate the impact of the number of classes in the classification scheme which
152 change in relation to the thematic resolution, we employed a recent typology of Tiwi Island
153 ecosystem types (Young *et al.*, 2024). This ecosystem typology was developed using the
154 GET and has a known relationship to each GET level. We tested classification schemes for
155 mapping at three levels of the GET hierarchy: the finest thematic resolution level 6
156 ‘subglobal ecosystem types’ with 11 classes, level 3 ‘ecosystem functional groups’ (EFGs)
157 with 10 classes, and level 2 ‘biome’ as the coarsest resolution with eight classes (Table 1).
158 Here we use the term ‘biome’ as defined by the GET; biomes represent the subdivision of
159 realms (e.g. fresh water) by similar broad features of ecosystem structure and function
160 (Keith *et al.*, 2022), although recognise other popular definitions (Mucina, 2019).

161 **2.3 Reference points**

162 Reference points (or ‘training points’) are confirmed occurrences of each ecosystem class
163 in the classification scheme. We employed the reference point collection developed in
164 (Young *et al.*, 2024) but describe the methods in more detail here.

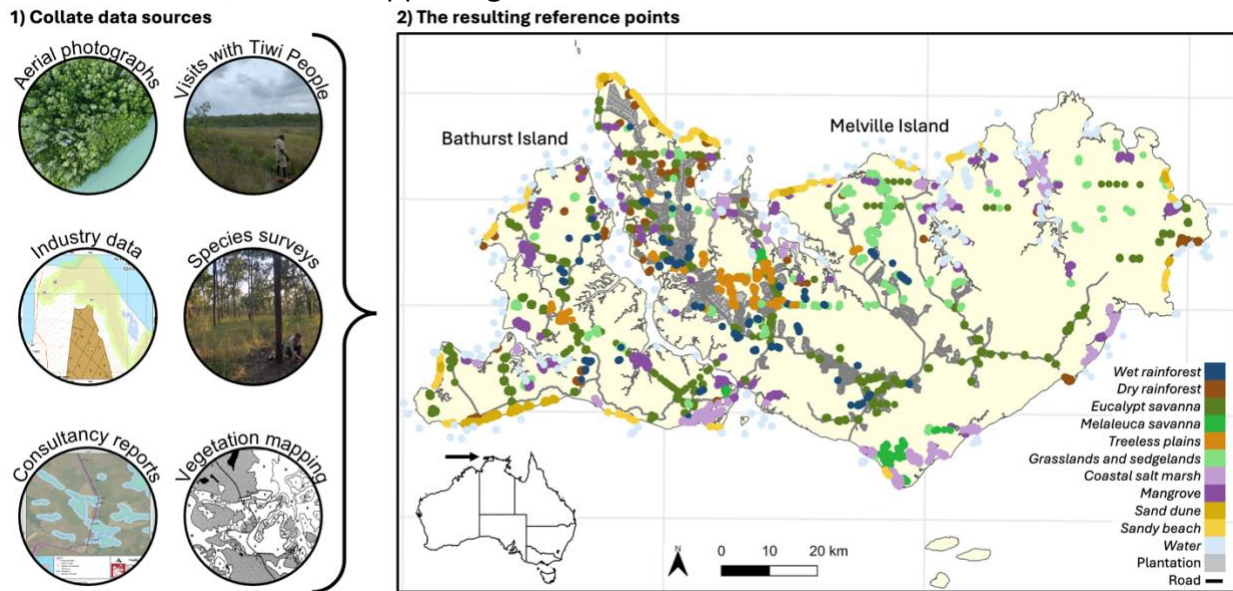
165 **2.3.1 Data collation**

166 We developed reference points from diverse spatial datasets available in a database
167 owned by the Tiwi Land Council, and field visits with Tiwi knowledge authorities (Table 1).
168 The spatial datasets incorporated data collected by numerous academic and industry
169 professionals over 35 years, and included various types of data, such as aerial
170 photographs, high-quality industry maps, and ecological surveys (Figure 1). For the aerial
171 photographs, we labelled each photograph with the ecosystems that were visible and
172 removed uncertain images. Aerial photographs provided essential information in remote
173 areas. We used GPS tracks and PDF maps from Tiwi Plantation Corporation to locate
174 rainforests and removed misclassifications identified in the field notes. These datasets
175 resulted in numerous reference points due to their high spatial accuracy. Consultancy
176 reports and development proposals contained vegetation maps and photographs, and
177 information regarding ecosystem processes (EcOz Environmental Services, 2012; EcOz
178 Environmental Consultants, 2021). Multiple academic datasets were available collected
179 by government and university academics and students. Rainforests were identified using
180 fauna, flora, and threatened species surveys (Russell-Smith, 1991; Menkhorst and
181 Woinarski, 1992; Gambold and Woinarski, 1993; Liddle and Elliott, 2008). *Eucalypt*

182 savannas have been surveyed for mammals and threatened fauna (Davies *et al.*, 2018,
 183 2019, 2021; Neave *et al.*, 2024). Vegetation communities of the *treeless plains* ecosystem
 184 (Wilson and Fensham, 1994) and *Melaleuca savanna* (Brocklehurst and Lynch, 2001, 2009)
 185 have been the focus of previous mapping efforts. However, developing reference points for
 186 the *treeless plains* maps was challenged by the low spatial detail in the line drawn maps
 187 and land use change since this time. From 2021 to 2023, we undertook on-ground visits
 188 with Tiwi knowledge authorities to locations and ecosystem types chosen by the Tiwi
 189 knowledge authorities.

190 **2.3.2 Reference point placement**

191 We placed initial reference points on a 30 m x 30 m grid at or near to the locations
 192 identified in the collated datasets through visual interpretation with recent Sentinel-2 and
 193 Landsat-9 imagery (described in section 2.4) in QGIS (QGIS Development Team, 2018).
 194 From the initial reference points, we removed all points closer than 100 m to minimise
 195 spatial autocorrelation and inflated evaluation metrics (Stehman, 2009; Stehman and
 196 Foody, 2019) using the ‘enmSdmX’ package with R in R-studio (R Core Team, 2018; RStudio
 197 Team, 2020; Smith *et al.*, 2023). This process yielded 5,887 reference points for the
 198 remainder of the analysis (Table 1, Figure 1). We obtained too few reference points to map
 199 *rocky shorelines* as this ecosystem was only identified from visits with Tiwi knowledge
 200 authorities. None of the collated datasets distinguished marine and freshwater
 201 ecosystems, and hence have been modelled together as *water* in this research. For all
 202 software details, see the Supporting Information.



203 Figure 1. The types of data sources used to develop the reference points and the final
 204 reference point locations.
 205

206 Table 1. Details of how the ecosystem types were grouped into the ecosystem functional
 207 group and biome classification schemes according to the Global Ecosystem Typology, and
 208 the data sources employed for each class to develop the reference points.

Classification schemes				Data sources for each ecosystem								
Biome (Level 2)	Ecosystem Functional Group (Level 3)	Tiwi Island mapped ecosystem types (Level 6)	Tiwi Island ecosystem typology (Level 6)	Wildlife aerial survey photos	Visits with Tiwi knowledge authorities	Tiwi Plantation Corporation maps	Threatened species monitoring	Tiwi Plantation Corporation surveys	Consultancy reports	Vegetation mapping aerial photos	Targeted vegetation mapping	Shoreline erosion maps
T1 Tropical-subtropical forests biome (n = 1575)	T1.1 Tropical/Subtropical lowland rainforests (n = 433)	Wet rainforest (n = 433)	Wet rainforest	X	X	X	X	X				
	T1.2 Tropical/Subtropical dry forests and thickets (n = 1142)	Dry rainforest (n = 1142)	Dry rainforest	X	X	X			X			
T3 Shrublands and shrubby woodlands (n = 214)	T3.1 Seasonally dry tropical shrublands (n = 214)	Treeless plains (n = 214)	Treeless plains	X	X				X	X	X	
T4 Savannas and grasslands (n = 1023)	T4.2 Pyric tussock savannas (n = 1023)	Eucalypt savanna (n = 927)	Eucalypt open forest savanna	X	X		X			X		
		<i>Melaleuca</i> savanna (n = 96)	<i>Melaleuca</i> savanna	X						X	X	
TF1 Palustrine wetlands biome (n = 704)	TF1.4 Seasonal floodplain marshes (n = 704)	Grasslands and sedgeland (n = 704)	Grasslands and sedgeland	X								
MFT1 Brackish tidal (n = 998)	MFT1.2 Intertidal forests and shrublands (n = 698)	Mangroves (n = 698)	Mangroves	X	X					X		
	MFT1.3 Coastal saltmarshes and reedbeds (n = 300)	Coastal saltmarsh (n = 300)	Coastal saltmarsh	X	X							
MT1 Shorelines biome (n = 428)	MT1.3 Sandy shorelines (n = 428)	Shorelines (n = 428)	Sandy beaches	X	X				X			X
			Rocky shorelines		X							
MT2 Supralittoral coastal biome (n = 531)	MT2.1 Coastal shrublands and grasslands (n = 531)	Sand dunes (n = 531)	Sand dunes		X				X			X
Water (n = 414)	Water (n = 414)	Water (n = 414)	Ocean	X	X							X
			Freshwater									

209 **2.4 Satellite image processing**

210 To test the impact of the choice in sensor and satellite image, we retrieved images
 211 acquired by the OLI-2 sensor onboard the Landsat-9 satellite (level 2, collection 2, tier 1),
 212 courtesy of the United States Geological Survey, and the MSI sensor on the Sentinel-2

213 satellite from the surface reflectance harmonised collection (level-2A) with atmospheric
214 correction, courtesy of the European Space Agency. In this paper, we refer to these two
215 data sources as ‘Landsat-9’ and ‘Sentinel-2’ for succinctness, recognising that each
216 satellite also represents different sensors, wavelengths measured, return times, and other
217 attributes. We obtained and processed the images using Google Earth Engine via the ‘rgee’
218 and ‘rgeeExtra’ packages in R (Gorelick *et al.*, 2017; Aybar *et al.*, 2020). For more details,
219 see the Supporting Information.

220
221 Clouds and smoke are common above the Tiwi islands. We tested multiple approaches for
222 developing cloud-free images suitable for modelling. We compiled image sets based on
223 the starting date (January, February, or March) and ending date (April or May) to capture
224 images prior to prescribed burning, from one year (2023), two years (2022 and 2023), or
225 three years (2021 to 2023). During the 2021 to 2023 period when the images were acquired,
226 there were no known changes in the extent of natural ecosystems and targeted
227 investigations supplementary to this research showed only localised changes in
228 mangroves which is not discussed further in this paper. We filtered the image sets by four
229 cloud cover limits (20%, 30%, 40% and 50%), masked the remaining clouds (see
230 Supporting Information for methods) and then reduced the image sets to a single image by
231 the median value of each pixel. We inspected the resultant 120 images for residual clouds.
232 We selected the method that minimised 1) the residual cloud, 2) the number of years, and
233 3) the cloud cover limit to include the most images.

234
235 The final Landsat-9 composite image was developed as the median of pixels from images
236 acquired over January to May in 2023 with less than 30% cloud cover. The final Sentinel-2
237 image was a three-year composite (2021 to 2023) of images acquired from January to May
238 each year with less than 20% cloud cover.

239 **2.5 Environmental covariates**

240 To develop covariates for testing, we extracted four bands for the red, green, blue, and
241 near-infrared wavelengths from the two satellite images and calculated the normalised
242 difference vegetation index (NDVI). For the additional covariates we obtained soil
243 composition layers from the Soil and Landscape Grid of Australia (Viscarra Rossel *et al.*,
244 2015) and calculated a mean for each layer in the top 30 cm and 2 m of soil. We obtained
245 elevation data from the Shuttle Radar Topography Mission (SRTM) 5-m Smoothed Digital
246 Elevation Model (DEM-S) (Gallant *et al.*, 2009) and created the Topographic Roughness
247 Index and slope (in degrees) using the ‘terra’ package (Hijmans, 2023). We also
248 investigated the height above which 50%, 75% and 95% of the vegetation biomass exists
249 (Scarth *et al.*, 2023). Data sources and detailed descriptions are available in the Supporting
250 Information.

251
252 To predict the ecosystem distribution across an area with the model, the covariate rasters
253 for each predictor must be available spatially, in the same resolution, and same
254 projection. We resampled the covariates using bilinear interpolation to the resolution of
255 the visible bands of each satellite (~30 m for OLI-2 sensor on the Landsat-9 satellite and

256 ~10 m for MSI sensor on the Sentinel-2 satellite) and the GDA2020 MGA52S coordinate
257 reference system (EPSG: 7852).

258
259 Correlations among predictor covariates are known to bias inference and affect parameter
260 estimates (Dormann *et al.*, 2013). We tested collinearity using Pearson’s correlation
261 coefficient, retaining covariates with pairwise correlations of less than 0.7 (Supporting
262 Information). For the satellite image covariate set, we retained red, near-infrared, and
263 NDVI. For the satellite image and additional covariate set, we retained red, near-infrared,
264 NDVI, elevation, slope, height of 50% of the vegetation biomass, and the organic carbon,
265 silt and clay in the top 30 cm of soil.

266 **2.6 Model formulation and fitting**

267 We tested 12 model formulations consisting of combinations of three modelling decisions.
268 For the three classification schemes, two satellites, and two covariate sets (total of 12
269 formulations), we fitted supervised, pixel-based random forest classification models
270 weighting each class by the number of reference points using the ‘ranger’ package (Wright
271 and Ziegler, 2017). We parameterised the models by testing the number of trees from 10 to
272 200 in intervals of 10, the number of covariates options to split the nodes from one to five,
273 and a tree depth of the even numbers from two to 10 as well as one. The optimal
274 parameters were 110 trees, two splitting covariates, and six node depth, and we employed
275 these parameter settings across all models for consistency. After parameterisation, we
276 fitted models for the 12 formulations using a cross-validation procedure. We randomly
277 assigned the reference points to one of five partitions, built the cross-validated models on
278 four of the five partitions and tested on the held-out partition for a total of 60 models.

279 **2.7 Model evaluation**

280 From the cross-validated models, we extracted the variable importance by the
281 permutation and summed the predicted classes for the held-out partition to produce a
282 confusion matrix. From the confusion matrices, we calculated the overall evaluation
283 metrics of the accuracy and kappa, and obtained the out-of-bag error from the model
284 output. We report on kappa because it remains prevalent in the literature (Morales-
285 Barquero *et al.*, 2019), despite known problems (Pontius Jr and Millones, 2011; Foody,
286 2020). We used the by-class evaluation metrics of sensitivity, specificity, precision, F1,
287 and negative predicted value. All evaluation metrics were calculated using the ‘caret’
288 package (Kuhn, 2008) using the equations in the Supporting Information. We tested the
289 sensitivity of the overall model evaluation metrics to the cross-validation procedure by
290 running 10,000 models for each formulation on a random 80% of the data and predicting to
291 the remaining 20%.

292 **2.8 Model prediction**

293 To map the spatial distribution of ecosystems, we predicted the probability of each class
294 for every pixel using the cross-validated models. The per-pixel probability is the proportion
295 of random forest trees that assigned the pixel to the class. The class with the highest
296 probability is the final predicted class for that pixel. We identified the predicted class for

297 each model formulation as the mode of the most probable class from the cross-validated
298 models. When multiple classes were predicted in equal amounts, we selected the class
299 with the highest mean probability. We then visualised the predicted class to map
300 ecosystem distribution and overlaid maps of the modified areas.

301 **2.9 Spatially explicit prediction confidence**

302 To communicate the reliability of the mapped spatial distributions, we demonstrate the
303 use of three spatially explicit evaluation metrics. Across the cross-validated models for
304 each pixel, we calculated the mean probability of the highest class (henceforth, maximum
305 probability; McIver and Friedl, 2001; Loosvelt *et al.*, 2012), the mean difference between
306 the highest and second highest probabilities (henceforth, ‘Margin of Victory’, MoV; McIver
307 and Friedl, 2001) and the number of unique predicted classes (henceforth, prediction
308 stability; (Grimmett, Whitsed and Horta, 2020). Both the maximum probability and the MoV
309 express the strength of the class assignment compared to the other class options. The
310 prediction stability indicates the repeatability within replicates of the same algorithm.

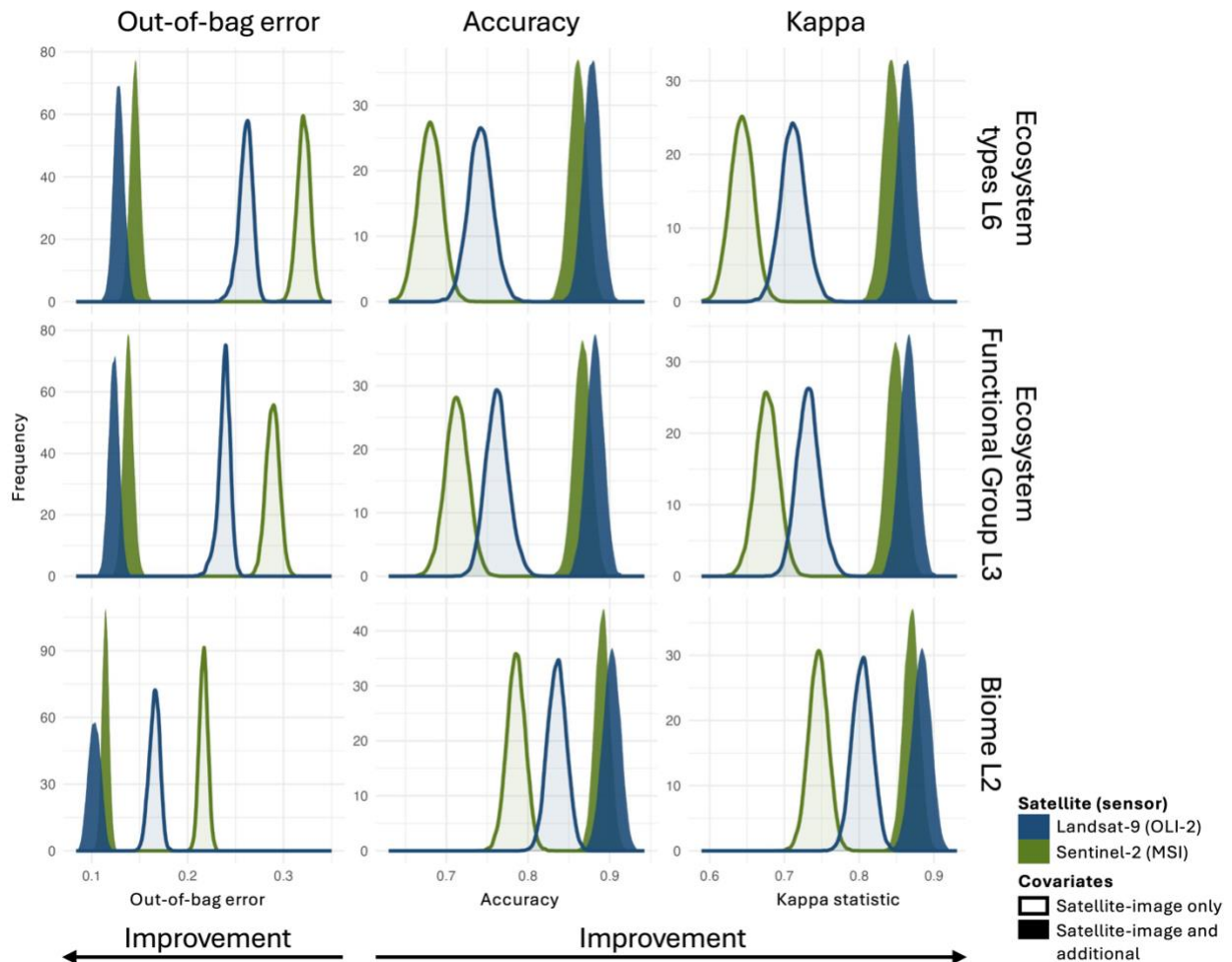
311 **3. Results**

312 We found that choice of covariates most strongly impacted model output. First, using the
313 satellite image and additional covariates together improved the overall evaluation metrics
314 across all model formulations (Figure 2 and Supporting Information). Most classes also
315 improved in by-class metrics (Figure 3) with few exceptions. The most pronounced
316 improvements were in the *treeless plains*, *Melaleuca savanna*, and the *wet* and *dry*
317 *rainforest* ecosystems (Figure 3 and Supporting Information). Not all additional covariates
318 contributed equally. On these relatively flat islands, elevation proved the most important
319 additional covariate, while the soil covariates and slope added little explanatory power
320 (Supporting Information).

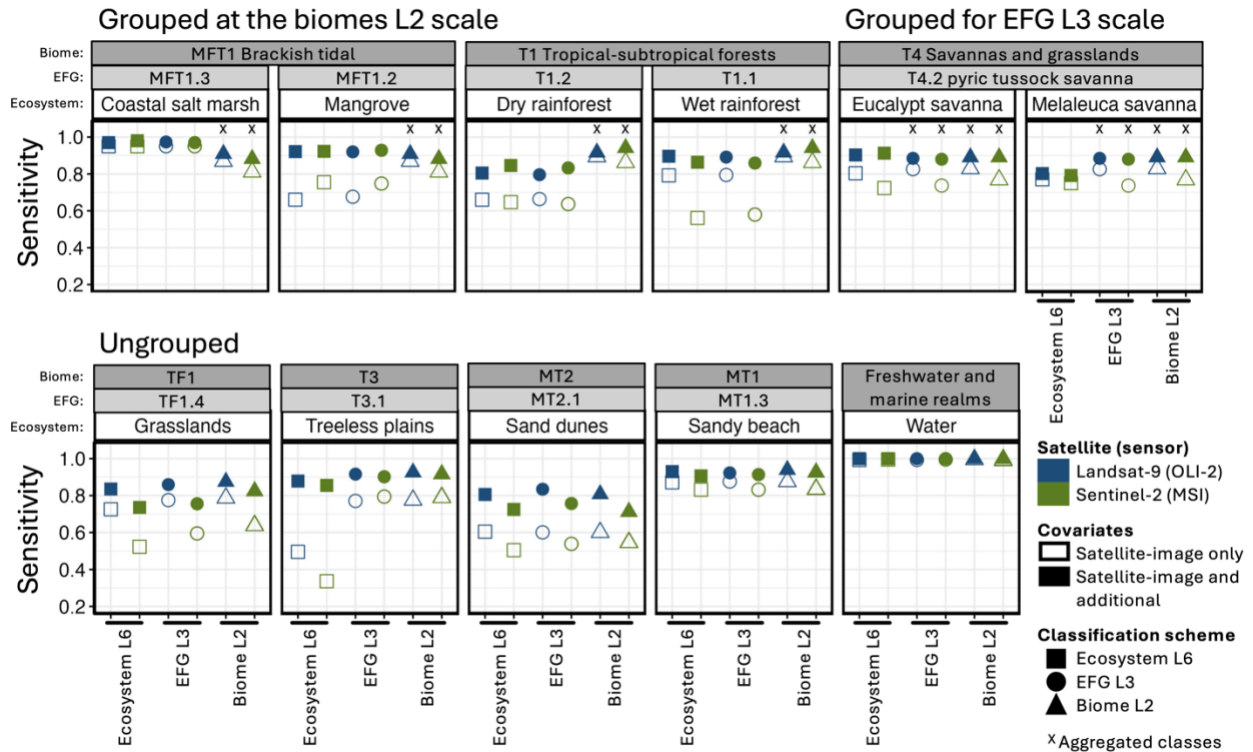
321
322 The satellite from which the satellite image was acquired was the second most influential
323 modelling decision. The models that used the Landsat-9 satellite image achieved higher
324 overall accuracy than those models using the Sentinel-2 image (Figure 2, and Supporting
325 Information). The effect of the satellite was most pronounced when only the satellite-
326 image covariates were used. With additional covariates, the Landsat-9 satellite image still
327 improved model performance, although to a lesser degree (Figure 2). Landsat-9 also
328 produced high by-class accuracies; however, the effect varied (Figure 3). For example, the
329 *dry* and *wet rainforests* showed by-class improvements with images acquired from the
330 Sentinel-2 satellite (Figure 3, and Supporting Information).

331
332 The classification scheme was the least impactful modelling decision that we tested on
333 the evaluation metrics. The biome classes (the coarsest grouping) slightly improved the
334 overall evaluation metrics, compared to the ecosystem and ecosystem functional groups
335 (Figure 2). This effect was less pronounced with the combined satellite and additional
336 covariates, and for images acquired from the Sentinel-2 satellite (Figure 2, and Supporting
337 Information). In general, the biome classification scheme did not change the by-class
338 evaluation estimates (Figure 3), the exception being the *wet* and *dry rainforest* ecosystem

339 types which were often misclassified in other classification schemes (Supporting
 340 Information).



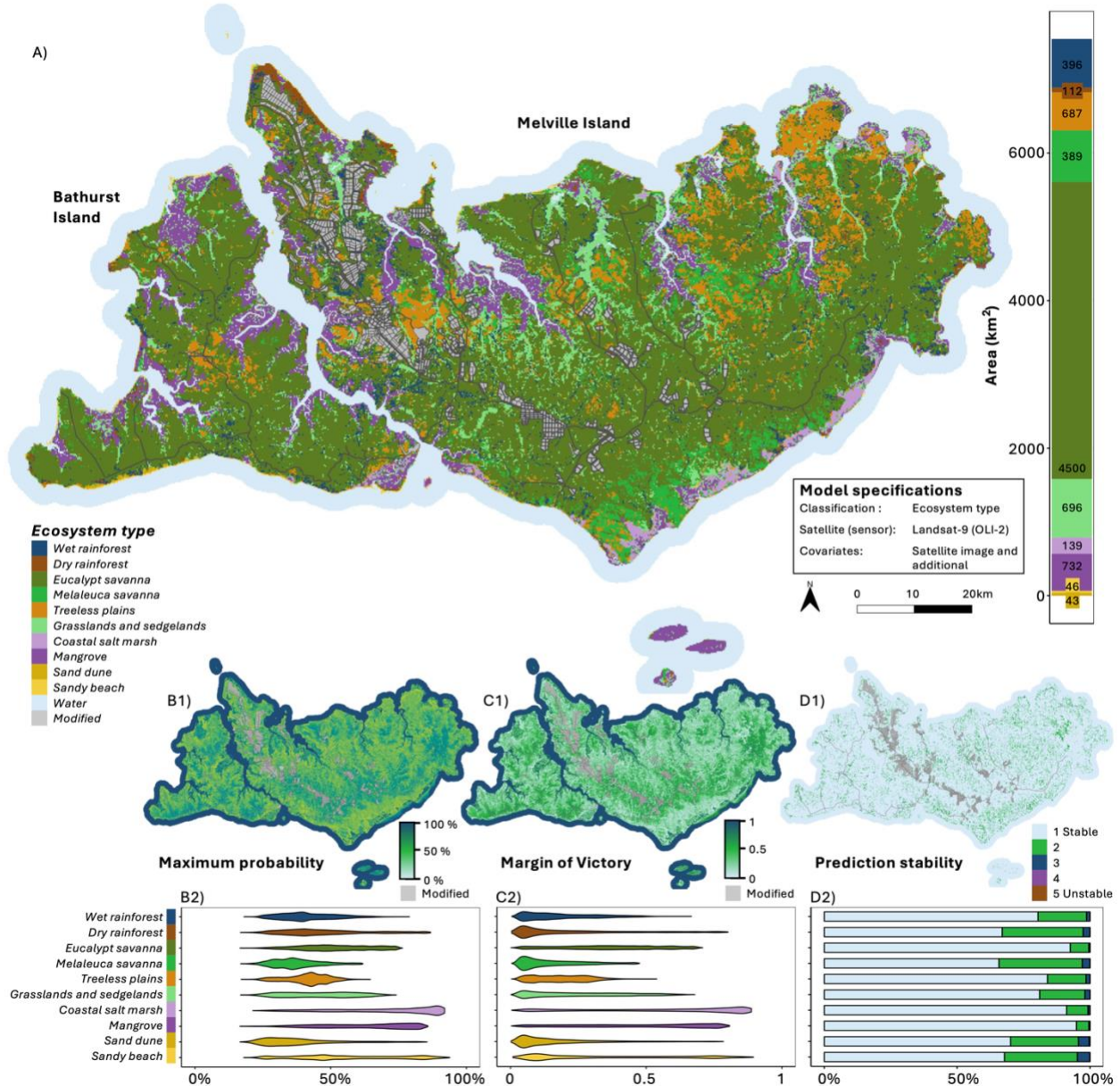
341
 342 Figure 2. The distribution of the overall evaluation metrics using out-of-bag error (left),
 343 accuracy (centre) and kappa statistic (right) from 10,000 random forest models built on
 344 80% of the data, where the model formulations varied by the classification scheme (row),
 345 covariates (fill) and satellite (colour).



346
 347 Figure 3. The by-class sensitivity as an exemplar evaluation metric for each class (panels)
 348 by the classification schemes (shape), satellite (colour), and covariates (fill). Ecosystem
 349 types that were aggregated into ecosystem functional groups (EFGs, data: circle, label:
 350 light grey box) and biomes (data: triangle, label: dark grey box above) are identified by an x.
 351 Sensitivity is the ability of the model to correctly predict the true class from all those known
 352 to be true in the reference points.

353 The maximum probability and MoV maps imply similar patterns of prediction confidence
 354 (Figure 4.B1 and C1). Areas with high confidence occur in a central band and eastern patch
 355 on Melville Island, and in isolated areas of Bathurst Island. Low confidence areas,
 356 including low stability in the prediction (Figure 4.D1), are scattered across the landscape
 357 with an aggregation on the southern coast and far east area of Melville Island.
 358 Summarising the prediction confidence across the entire area (Figure 4.B2-D2), the
 359 *coastal salt marsh* (light purple) and *mangrove* (dark purple) were predicted with highest
 360 confidence (median maximum probability = 75.72% and 64.77%, respectively, and median
 361 Mov = 66.15% and 50.46%), indicated by the distribution of the maximum probability and
 362 MoV skewed to the right (Figure 4.B2-C2). *Mangroves* were also the most stable ecosystem
 363 type with 94.86% of the cells mapped as mangroves only ever predicted to be mangroves,
 364 followed by *eucalypt savanna* at 92.57% (Figure 4.D2, light blue boxes). *Sand dunes* were
 365 predicted with the low maximum probability values (median of 34.82%) indicated by the
 366 distribution skewed to the left (Figure 4.B2, dark yellow), while the MoV distribution is low
 367 (median of 11.89%) but comparable to other classes (Figure 4.C2). *Sand dunes* and *sandy*
 368 *beaches* produced unstable predictions with the highest proportion of cells predicted as
 369 three different classes (4.65% and 4.03%, Figure 4.D2 dark blue bar), followed by

370 *melaleuca savanna* and *dry rainforests* with the highest proportion of cells with two
 371 classes (31.35% and 30.46%, Figure 4.D2 green bar).



372
 373 Figure 4. The predicted ecosystem map (A) and spatially explicit evaluation metrics (B-D)
 374 for an example model using the ecosystem type as the classification scheme, imagery
 375 from the Landsat-9 satellite, and additional covariate alongside those from the satellite
 376 image.

377 4. Discussion

378 We found that decisions made during the ecosystem mapping procedure strongly
 379 impacted model outputs (Figure 2 and Figure 3), consistent with previous studies
 380 (Simensen *et al.*, 2020; Trouvé *et al.*, 2023; Naas *et al.*, 2024). The combination of satellite

381 image and additional covariates greatly improved the model performance, supporting
382 previous calls to ensure that ecosystem models capture key attributes of ecosystems and
383 are developed with ecosystem scientists (Xiao *et al.*, 2024). Since we found that the choice
384 of satellite and classification scheme were less influential, additional elements can be
385 considered to guide the decision; Landsat has the advantage of a longer archive, allowing
386 mapping of change through time, while mapping finer ecosystem units has benefits for
387 management of biodiversity.

388
389 Ecological theory posits that the distribution of biodiversity is shaped by environmental
390 gradients. Our results showed that the best predictions came from a model including both
391 satellite and additional covariates, aligning with previous research (Simensen *et al.*, 2020;
392 Trouvé *et al.*, 2023; Naas *et al.*, 2024). The elevation covariate added the most explanatory
393 power (Supporting Information), potentially as a proxy for other ecological gradients and
394 processes (Whittaker, 1956). Topographic covariates representing water availability are
395 often valuable to distinguish wet and dry forest types, including rainforests and riparian
396 forests (Trouvé *et al.*, 2023). While the additional covariates contributed useful
397 information, we found that the satellite covariates were still highly informative (Supporting
398 Information), congruent with other studies that suggest ecological or climate covariates
399 are best used alongside covariates from other sources, particularly satellite imagery
400 (Simensen *et al.*, 2020; Trouvé *et al.*, 2023; Naas *et al.*, 2024). Soil covariates were the least
401 informative in this study (Supporting Information), potentially due to underlying data
402 inaccuracies in the available dataset, as noted in other global and national soil maps
403 (Rossiter *et al.*, 2022; Maynard *et al.*, 2023), rather than a lack of ecological importance
404 (Simensen *et al.*, 2020; Keith *et al.*, 2022). Improving the availability, accessibility, and
405 spatiotemporal resolution of ecological covariates would improve both the map reliability
406 and our understanding of the environmental gradients defining their extent. Once such
407 covariates are available, deep learning models, reproducible workflows, and infrastructure
408 are critical to interrogate such large datasets and offer novel insights (Galaz García *et al.*,
409 2023; Pettorelli *et al.*, 2024).

410
411 In addition to the model covariates, the choice of the satellite also influenced model
412 performance. We found that the Landsat-9 satellite imagery generally provided higher
413 overall (Figure 2) and by-class evaluation metrics (Figure 3), although the effect lessens
414 with the inclusion of additional covariates. Exceptions to this were the *wet* and *dry*
415 *rainforest* ecosystem types, where we detected improvements with the Sentinel-2 satellite
416 image (Figure 3). The Sentinel-2 satellite imagery with the MSI sensor capture finer spatial
417 resolution imagery and may better detect the sharp boundaries that delineate rainforests,
418 reducing the number of pixels containing multiple ecosystem types (i.e. mixed pixels).
419 Mixed pixels are a high source of uncertainty in landcover mapping (Loosvelt *et al.*, 2012)
420 and hamper the reliability of global and national maps (Herold *et al.*, 2008; Congalton *et*
421 *al.*, 2014).

422
423 Alternatively, high spatial resolution sensors may detect structural variability within
424 ecosystem classes, leading to high intra-class variability and noise (Nagendra and

425 Rocchini, 2008). For instance, savanna ecosystems display highly variable tree occurrence
426 and canopy cover (Keith *et al.*, 2022). In general, satellite spatial resolution has no
427 consistent effect on map reliability (Yu *et al.*, 2014; Morales-Barquero *et al.*, 2019). This
428 suggests that management objectives and ecosystem characteristics should determine
429 the satellite and sensor used (Horvath *et al.*, 2021; Venter *et al.*, 2022; Naas *et al.*, 2024).
430 The additional benefit of the Landsat satellites is the rich archive of images (Wulder *et al.*,
431 2012) and hence the potential to detect historical changes (Murray *et al.*, 2019; Calderón-
432 Loor, Hadjidakou and Bryan, 2021).

433

434 While here we have described the potential effect that spatial resolution may have on
435 ecosystem mapping, we cannot disentangle this effect from the other differences between
436 the Landsat-9 and Sentinel-2 missions. Satellite missions vary in many attributes,
437 including the return time influencing the number of images captured, spectral resolution
438 such as acquiring hyperspectral imagery, and the presence of other instruments with
439 unique data captured such as synthetic aperture radar (Pettorelli *et al.*, 2014). These
440 differences are particularly important in tropical regions where obtaining an image with
441 limited cloud and smoke cover is challenging, as experienced in this research. As we
442 compiled cloud-free composite images from images taken over a period of time, there is a
443 risk of intra- and inter-annual change. In locations with high rates of landscape change,
444 composite images require careful use and would reduce the map reliability.

445

446 The least influential modelling decision was the classification scheme, where the overall
447 evaluation metrics were slightly improved with the GET level 2 ‘biome’ scale representing
448 the fewest classes and coarsest scale of biodiversity. Aggregating classes is a common
449 method to improve evaluation metrics (Congalton and Green, 1993; Remmel, 2009) but
450 overall, the benefits are small and variable (Yu *et al.*, 2014). Importantly, modelling biomes
451 presents a direct trade-off with usefulness for future applications where the finer scale
452 classification of ecosystems types is fundamental to management, such as with
453 ecosystem accounting and ecological risk assessments (Hein *et al.*, 2020; Keith, Ferrer-
454 Paris, *et al.*, 2024). The improvements we observed were driven by aggregating specific
455 classes that were often misclassified, namely the *wet* and *dry rainforest*. Such rainforest
456 ecosystems are both represented by the GET level 2 ‘tropical and subtropical forests
457 biome’ but globally these ecosystems differ in threat status (Etter *et al.*, 2017; Murray *et al.*,
458 2020; Noh *et al.*, 2020) and protection (Wohlfart, Wegmann and Leimgruber, 2014;
459 Rivas, Guerrero-Casado and Navarro-Cerillo, 2021). Aggregating and mapping these
460 ecosystems at the biome scale obscures the urgency and practicality of protecting and
461 managing the world’s tropical forests.

462

463 Thoughtful model formulation can reduce but never remove error and uncertainty in the
464 model outputs (Rocchini *et al.*, 2013; Foody, 2021). As demonstrated here, spatially
465 explicit prediction confidences are immediate tools that can be readily implemented to
466 communicate spatial patterns of reliability in the maps. Our analysis produced generally
467 low confidence metrics with broadly consistent spatial patterns across the metrics (Figure
468 4). There are multiple reasons which may lead to the lower confidence predictions (Elith,

469 Burgman and Regan, 2002; Regan, Colyvan and Burgman, 2002). The model may poorly
470 define and predict classes due to a lack of relevant covariates or measurement errors in
471 these covariate layers (Elith, Burgman and Regan, 2002; Barry and Elith, 2006), such as the
472 global soil maps described earlier (Rossiter *et al.*, 2022; Maynard *et al.*, 2023). Natural
473 variation within heterogeneous classes may drive the lower confidence predictions for the
474 *sand dunes* and *melaleuca savanna* which display high variation in grass and tree cover
475 (Young *et al.*, 2024). Ecotones, mixed pixels, or too few reference points often produce
476 poor accuracy (Loosvelt *et al.*, 2012; Rocchini *et al.*, 2013; Foody, 2022). The exact metrics
477 of prediction confidence depend on the model type and warrants research for emerging
478 machine learning models (Pettorelli *et al.*, 2024).

479

480 **Conclusion**

481 Ecosystem maps tend to be presented without a discussion of the decisions made during
482 the modelling processes nor an evaluation of the implications of these decisions. As new
483 avenues in broad-scale monitoring and change detection of ecosystems arise (Galaz
484 García *et al.*, 2023; Pettorelli *et al.*, 2024), the need to carefully examine the impact of
485 modelling decisions grows. Given the influence of modelling decisions that we identified,
486 both modellers and users must continue to be aware of the role model formulation plays in
487 ecosystem mapping and endeavour to account for map reliability in future applications.
488 Incorporating uncertainty into decision-making is paramount, albeit not always
489 straightforward (Burgman, Lindenmayer and Elith, 2005). The responsibility lies on both the
490 producer of any map to communicate reliability in ways transferable to future applications,
491 and on the user to propagate known uncertainties.

492 **Acknowledgements**

493 We acknowledge the extensive work undertaken by previous researchers, consultants, and
494 industry professionals in developing their respective datasets and products which allowed
495 the creation of the reference points for this research. The Tiwi Islands are the lands of the
496 Tiwi people from eight land-owning clans: Jikilaruwu, Malawu, Mantiyupwi,
497 Marrikawuyanga, Munupi, Wulirankuwu, Wurankuwu, and Yimpinari. We would like to
498 thank Mavis Kerinauia, Colin Kerinauia, Simon Munkara, Bernard Tipoloura, Gemma
499 Munkara, John Louis Munkara, Kinjia Munkara-Murray and Marie Munkara for visiting
500 locations on the Tiwi Islands. We thank Mavis Kerinariauia, Alana Brekelmans, Margaret
501 Ayre, Michaela Spencer, the Tiwi Land Council, Tiwi Resources, and Tiwi rangers for their
502 involvement and facilitation during on-ground visits. Analysis and writing were undertaken
503 on the lands of the Wurundjeri Woi Wurung peoples of the Kulin Nation.

504 **Conflict of interest statement:**

505 The authors disclose no conflict of interest.

506 **Ethics statement:**

507 Human ethics was approved by The University of Melbourne Human Ethics (#1955248) and
508 Deakin University Human Research Ethics Committee (#2022097). Permission to enter the

509 Tiwi Islands, to view the satellite imagery, and access the datasets for the training points
510 was granted by the Tiwi Land Council.

511 **Funding statement:**

512 This research was funded by the Australian Research Council (ARC) linkage grant
513 (LP170100305) in partnership with the Tiwi Land Council. The field visits with Tiwi
514 knowledge authorities was funded by the Foundation for National Parks and Wildlife
515 community conservation grant (FNPW028CCG22).

516 **References**

517 Aybar, C., Wu, Q., Bautista, L., Yali, R. and Barja, A. (2020) 'rgee: An R package for
518 interacting with Google Earth Engine', *Journal of Open Source Software*, 5(51), p. 2272.
519 Available at: <https://doi.org/10.21105/joss.02272>.

520 Barry, S. and Elith, J. (2006) 'Error and uncertainty in habitat models', *Journal of Applied*
521 *Ecology*, 43(3), pp. 413–423. Available at: [https://doi.org/10.1111/j.1365-](https://doi.org/10.1111/j.1365-2664.2006.01136.x)
522 [2664.2006.01136.x](https://doi.org/10.1111/j.1365-2664.2006.01136.x).

523 Brocklehurst, P. and Lynch, B. (2009) *Northern Territory Melaleuca forest survey*. Technical
524 Report 25/2009D. Palmerston, Northern Territory: Department of Natural Resources,
525 Environment, The Arts and Sport.

526 Brocklehurst, P. and Lynch, D. (2001) *Melaleuca Survey of the Top End, Northern Territory*.
527 Technical Report 25/2009D. Palmerston, Northern Territory: Department of Natural
528 Resources, Environment, The Arts and Sport, p. 89.

529 Burgman, M.A., Lindenmayer, D.B. and Elith, J. (2005) 'Managing Landscapes for
530 Conservation Under Uncertainty', *Ecology*, 86(8), pp. 2007–2017. Available at:
531 <https://doi.org/10.1890/04-0906>.

532 Calderón-Loor, M., Hadjikakou, M. and Bryan, B.A. (2021) 'High-resolution wall-to-wall
533 land-cover mapping and land change assessment for Australia from 1985 to 2015', *Remote*
534 *Sensing of Environment*, 252, p. 112148. Available at:
535 <https://doi.org/10.1016/j.rse.2020.112148>.

536 Capotorti, G., Del Vico, E., Copiz, R., Facioni, L., Zavattero, L., Bonacquisti, S., Paolanti, M.
537 and Blasi, C. (2023) 'Ecosystems of Italy. Updated mapping and typology for the
538 implementation of national and international biodiversity-related policies', *Plant*
539 *Biosystems - An International Journal Dealing with all Aspects of Plant Biology*, 157(6), pp.
540 1248–1258. Available at: <https://doi.org/10.1080/11263504.2023.2284135>.

541 CBD (1992) *Convention on biological diversity*. Rio de Janeiro: United Nations. Available at:
542 [https://treaties.un.org/doc/Treaties/1992/06/19920605%2008-](https://treaties.un.org/doc/Treaties/1992/06/19920605%2008-44%20PM/Ch_XXVII_08p.pdf)
543 [44%20PM/Ch_XXVII_08p.pdf](https://treaties.un.org/doc/Treaties/1992/06/19920605%2008-44%20PM/Ch_XXVII_08p.pdf).

- 544 Congalton, R.G. and Green, K. (1993) 'A practical look at the sources of confusion in error
545 matrix generation.', *Photogrammetric engineering and remote sensing*, 59(5), pp. 641–644.
- 546 Congalton, R.G., Gu, J., Yadav, K., Thenkabail, P. and Ozdogan, M. (2014) 'Global Land
547 Cover Mapping: A Review and Uncertainty Analysis', *Remote Sensing*, 6(12), pp. 12070–
548 12093. Available at: <https://doi.org/10.3390/rs61212070>.
- 549 Davies, H.F., McCarthy, M.A., Firth, R.S.C., Woinarski, J.C.Z., Gillespie, G.R., Andersen,
550 A.N., Rioli, W., Puruntatameri, J., Roberts, W., Kerinauia, C., Kerinauia, V., Womatakimi,
551 K.B. and Murphy, B.P. (2018) 'Declining populations in one of the last refuges for
552 threatened mammal species in northern Australia', *Austral Ecology*, 43(5), pp. 602–612.
553 Available at: <https://doi.org/10.1111/aec.12596>.
- 554 Davies, H.F., Rangers, T.L., Rees, M.W., Stokeld, D., Miller, A.C., Gillespie, G.R. and
555 Murphy, B.P. (2021) 'Variation in feral cat density between two large adjacent islands in
556 Australia's monsoon tropics', *Pacific Conservation Biology*, 28(1), pp. 18–24. Available at:
557 <https://doi.org/10.1071/PC20088>.
- 558 Davies, H.F., Rioli, W., Puruntatameri, J., Roberts, W., Kerinauia, C., Kerinauia, V.,
559 Womatakimi, K.B., Gillespie, G.R. and Murphy, B.P. (2019) 'Estimating site occupancy and
560 detectability of the threatened partridge pigeon (*Geophaps smithii*) using camera traps',
561 *Austral Ecology*, 44(5), pp. 868–879. Available at: <https://doi.org/10.1111/aec.12755>.
- 562 DCCEEW (2021) 'Interim Biogeographic Regionalisation for Australia (IBRA)'.
- 563 De la Cruz, M., Quintana-Ascencio, P.F., Cayuela, L., Espinosa, C.I. and Escudero, A.
564 (2017) 'Comment on "The extent of forest in dryland biomes"', *Science* [Preprint]. Available
565 at: <https://doi.org/10.1126/science.aao0369>.
- 566 Dormann, C.F., Elith, J., Bacher, S., Buchmann, C., Carl, G., Carré, G., Marquéz, J.R.G.,
567 Gruber, B., Lafourcade, B., Leitão, P.J., Münkemüller, T., McClean, C., Osborne, P.E.,
568 Reineking, B., Schröder, B., Skidmore, A.K., Zurell, D. and Lautenbach, S. (2013)
569 'Collinearity: a review of methods to deal with it and a simulation study evaluating their
570 performance', *Ecography*, 36(1), pp. 27–46. Available at: <https://doi.org/10.1111/j.1600-0587.2012.07348.x>.
- 572 Dorrough, J., Tozer, M., Armstrong, R., Summerell, G. and Scott, M.L. (2021) 'Quantifying
573 uncertainty in the identification of endangered ecological communities', *Conservation
574 Science and Practice*, 3(11), p. e537. Available at: <https://doi.org/10.1111/csp2.537>.
- 575 Dryflor, Banda-R, K., Delgado-Salinas, A., Dexter, K.G., Linares-Palomino, R., Oliveira-
576 Filho, A., Prado, D., Pullan, M., Quintana, C., Riina, R., Rodríguez M., G.M., Weintritt, J.,
577 Acevedo-Rodríguez, P., Adarve, J., Álvarez, E., Aranguren B., A., Arteaga, J.C., Aymard, G.,
578 Castaño, A., Ceballos-Mago, N., Cogollo, Á., Cuadros, H., Delgado, F., Devia, W., Dueñas,
579 H., Fajardo, L., Fernández, Á., Fernández, M.Á., Franklin, J., Freid, E.H., Galetti, L.A., Gonto,

580 R., González-M., R., Graveson, R., Helmer, E.H., Idárraga, Á., López, R., Marcano-Vega, H.,
581 Martínez, O.G., Maturo, H.M., McDonald, M., McLaren, K., Melo, O., Mijares, F., Mogni, V.,
582 Molina, D., Moreno, N.D.P., Nassar, J.M., Neves, D.M., Oakley, L.J., Oatham, M., Olvera-
583 Luna, A.R., Pezzini, F.F., Dominguez, O.J.R., Ríos, M.E., Rivera, O., Rodríguez, N., Rojas, A.,
584 Särkinen, T., Sánchez, R., Smith, M., Vargas, C., Villanueva, B. and Pennington, R.T. (2016)
585 ‘Plant diversity patterns in neotropical dry forests and their conservation implications’,
586 *Science*, 353(6306), pp. 1383–1387. Available at: <https://doi.org/10.1126/science.aaf5080>.

587 EcOz Environmental Consultants (2021) *Terrestrial Ecology Report - Tiwi Islands H2*
588 *Project. Provaris Energy*,. Report for Provaris Energy. Darwin, Northern Territory.

589 EcOz Environmental Services (2012) *Kilimiraka Notice of Intent: Kilimiraka Mineral Sands*
590 *Project, Bathurst Island, N.T.* Report for Matilda Zircon.

591 Elith, J., Burgman, M.A. and Regan, H.M. (2002) ‘Mapping epistemic uncertainties and
592 vague concepts in predictions of species distribution’, *Ecological Modelling*, 157(2), pp.
593 313–329. Available at: [https://doi.org/10.1016/S0304-3800\(02\)00202-8](https://doi.org/10.1016/S0304-3800(02)00202-8).

594 Etter, A., Andrade, Á., Saavedra, K., Amaya, P. and Arévalo, P. (2017) *Estado de los*
595 *Ecosistemas Colombianos: una aplicación de la metodología de la Lista Roja de*
596 *Ecosistemas (Vers2.0)*. Bogota, Colombia: Pontificia Universidad Javeriana y Conservación
597 InternacionalColombia, p. 138. Available at:
598 [https://www.conservation.org.co/media/A7.LRE-](https://www.conservation.org.co/media/A7.LRE-Colombia_INFORME%20FINAL_%202017.pdf)
599 [Colombia_INFORME%20FINAL_%202017.pdf](https://www.conservation.org.co/media/A7.LRE-Colombia_INFORME%20FINAL_%202017.pdf).

600 Foody, G.M. (2002) ‘Status of land cover classification accuracy assessment’, *Remote*
601 *Sensing of Environment*, 80(1), pp. 185–201. Available at: [https://doi.org/10.1016/S0034-](https://doi.org/10.1016/S0034-4257(01)00295-4)
602 [4257\(01\)00295-4](https://doi.org/10.1016/S0034-4257(01)00295-4).

603 Foody, G.M. (2020) ‘Explaining the unsuitability of the kappa coefficient in the assessment
604 and comparison of the accuracy of thematic maps obtained by image classification’,
605 *Remote Sensing of Environment*, 239, p. 111630. Available at:
606 <https://doi.org/10.1016/j.rse.2019.111630>.

607 Foody, G.M. (2021) ‘Impacts of ignorance on the accuracy of image classification and
608 thematic mapping’, *Remote Sensing of Environment*, 259, p. 112367. Available at:
609 <https://doi.org/10.1016/j.rse.2021.112367>.

610 Foody, G.M. (2022) ‘Global and Local Assessment of Image Classification Quality on an
611 Overall and Per-Class Basis without Ground Reference Data’, *Remote Sensing*, 14(21), p.
612 5380. Available at: <https://doi.org/10.3390/rs14215380>.

613 Galaz García, C., Bagstad, K.J., Brun, J., Chaplin-Kramer, R., Dhu, T., Murray, N.J., Nolan,
614 C.J., Ricketts, T.H., Sosik, H.M., Sousa, D., Willard, G. and Halpern, B.S. (2023) ‘The future
615 of ecosystem assessments is automation, collaboration, and artificial intelligence’,

616 *Environmental Research Letters*, 18(1), p. 011003. Available at:
617 <https://doi.org/10.1088/1748-9326/acab19>.

618 Gallant, J., Wilson, N., Tickle, P.K., Downling, T. and Read, A. (2009) ‘3 second SRTM
619 Derived Digital Elevation Model (DEM) Version 1.0.’ Canberra: Geoscience Australia.
620 Available at: <http://pid.geoscience.gov.au/dataset/ga/69888>.

621 Gambold, N. and Woinarski, J.C.Z. (1993) ‘Distributional patterns of herpetofauna in
622 monsoon rainforests of the Northern Territory, Australia’, *Australian Journal of Ecology*,
623 18(4), pp. 431–449. Available at: <https://doi.org/10.1111/j.1442-9993.1993.tb00470.x>.

624 Gorelick, N., Hancher, M., Dixon, M., Ilyushchenko, S., Thau, D. and Moore, R. (2017)
625 ‘Google Earth Engine: Planetary-scale geospatial analysis for everyone’, *Remote Sensing of*
626 *Environment*, 202, pp. 18–27. Available at: <https://doi.org/10.1016/j.rse.2017.06.031>.

627 Gould, E., Fraser, H.S., Parker, T.H., Nakagawa, S., Griffith, S.C., Vesk, P.A., Fidler, F.,
628 Hamilton, D.G., Abbey-Lee, R.N., Abbott, J.K., Aguirre, L.A., Alcaraz, C., Aloni, I., Altschul,
629 D., Arekar, K., Atkins, J.W., Atkinson, J., Baker, C., Barrett, M., Bell, K., Bello, S.K., Beltrán,
630 I., Berauer, B.J., Bertram, M.G., Billman, P.D., Blake, C.K., Blake, S., Bliard, L., Bonisoli-
631 Alquati, A., Bonnet, T., Bordes, C.N.M., Bose, A.P.H., Botterill-James, T., Boyd, M.A., Boyle,
632 S.A., Bradfer-Lawrence, T., Bradham, J., Brand, J.A., Brengdahl, M.I., Bulla, M., Bussière, L.,
633 Camerlenghi, E., Campbell, S.E., Campos, L.L.F., Caravaggi, A., Cardoso, P., Carroll,
634 C.J.W., Catanach, T.A., Chen, X., Chik, H.Y.J., Choy, E.S., Christie, A.P., Chuang, A.,
635 Chunco, A.J., Clark, B.L., Contina, A., Covernton, G.A., Cox, M.P., Cressman, K.A., Crotti,
636 M., Crouch, C.D., D’Amelio, P.B., Sousa, A.A. de, Döbert, T.F., Dobler, R., Dobson, A.J.,
637 Doherty, T.S., Drobniak, S.M., Duffy, A.G., Duncan, A.B., Dunn, R.P., Dunning, J., Dutta, T.,
638 Eberhart-Hertel, L., Elmore, J.A., Elsherif, M.M., English, H.M., Ensminger, D.C., Ernst,
639 U.R., Ferguson, S.M., Fernández-Juricic, E., Ferreira-Arruda, T., Fieberg, J., Finch, E.A.,
640 Fiorenza, E.A., Fisher, D.N., Fontaine, A., Forstmeier, W., Fourcade, Y., Frank, G.S.,
641 Freund, C.A., Fuentes-Lillo, E., Gandy, S.L., Gannon, D.G., García-Cervigón, A.I.,
642 Garretson, A.C., Ge, X., Geary, W.L., Géron, C., Gilles, M., Girndt, A., Gliksman, D.,
643 Goldspiel, H.B., Gomes, D.G.E., Good, M.K., Goslee, S.C., Gosnell, J.S., Grames, E.M.,
644 Gratton, P., Grebe, N.M., Greenler, S.M., Griffioen, M., Griffith, D.M., Griffith, F.J.,
645 Grossman, J.J., Günçan, A., Haesen, S., Hagan, J.G., Hager, H.A., Harris, J.P., Harrison,
646 N.D., Hasnain, S.S., Havird, J.C., Heaton, A.J., Herrera-Chaustre, M.L., Howard, T.J., Hsu,
647 B.-Y., Iannarilli, F., Iranzo, E.C., Iverson, E.N.K., Jimoh, S.O., Johnson, D.H., Johnsson, M.,
648 Jorna, J., Jucker, T., Jung, M., Kačergytė, I., Kaltz, O., Ke, A., Kelly, C.D., Keogan, K.,
649 Keppeler, F.W., Killion, A.K., Kim, D., Kochan, D.P., Korsten, P., Kothari, S., Kuppler, J.,
650 Kusch, J.M., Lagisz, M., Lalla, K.M., Larkin, D.J., Larson, C.L., Lauck, K.S., Lauterbur, M.E.,
651 Law, A., Léandri-Breton, D.-J., Lembrechts, J.J., L’Herpinier, K., Lievens, E.J.P., Lima, D.O.
652 de, Lindsay, S., Luquet, M., MacLeod, R., Macphie, K.H., Magellan, K., Mair, M.M., Malm,
653 L.E., Mammola, S., Mandeville, C.P., Manhart, M., Manrique-Garzon, L.M., Mäntylä, E.,
654 Marchand, P., Marshall, B.M., Martin, C.A., Martin, D.A., Martin, J.M., Martinig, A.R.,
655 McCallum, E.S., McCauley, M., McNew, S.M., Meiners, S.J., Merkling, T., Michelangeli, M.,

656 Moiron, M., Moreira, B., Mortensen, J., Mos, B., Muraina, T.O., Murphy, P.W., Nelli, L.,
657 Niemelä, P., Nightingale, J., Nilsson, G., Nolzco, S., Nooten, S.S., Novotny, J.L., Olin,
658 A.B., Organ, C.L., Ostevik, K.L., Palacio, F.X., Paquet, M., Parker, D.J., Pascall, D.J.,
659 Pasquarella, V.J., Paterson, J.H., Payo-Payo, A., Pedersen, K.M., Perez, G., Perry, K.I.,
660 Pottier, P., Proulx, M.J., Proulx, R., Pruett, J.L., Ramananjato, V., Randimbiarison, F.T.,
661 Razafindratsima, O.H., Rennison, D.J., Riva, F., Riyahi, S., Roast, M.J., Rocha, F.P., Roche,
662 D.G., Román-Palacios, C., Rosenberg, M.S., Ross, J., Rowland, F.E., Rugemalila, D.,
663 Russell, A.L., Ruuskanen, S., Saccone, P., Sadeh, A., Salazar, S.M., Sales, K., Salmón, P.,
664 Sánchez-Tójar, A., Santos, L.P., Santostefano, F., Schilling, H.T., Schmidt, M., Schmoll, T.,
665 Schneider, A.C., Schrock, A.E., Schroeder, J., Schtickzelle, N., Schultz, N.L., Scott, D.A.,
666 Scroggie, M.P., Shapiro, J.T., Sharma, N., Shearer, C.L., Simón, D., Sitvarin, M.I., Skupien,
667 F.L., Slinn, H.L., Smith, G.P., Smith, J.A., Sollmann, R., Whitney, K.S., Still, S.M., Stuber,
668 E.F., Sutton, G.F., Swallow, B., Taff, C.C., Takola, E., Tanentzap, A.J., Tarjuelo, R., Telford,
669 R.J., Thawley, C.J., Thierry, H., Thomson, J., Tidau, S., Tompkins, E.M., Tortorelli, C.M.,
670 Trlica, A., Turnell, B.R., Urban, L., Vondel, S.V. de, Wal, J.E.M. van der, Eeckhoven, J.V.,
671 Oordt, F. van, Vanderwel, K.M., Vanderwel, M.C., Vanderwolf, K.J., Vélez, J., Vergara-
672 Florez, D.C., Verrelli, B.C., Vieira, M.V., Villamil, N., Vitali, V., Vollering, J., Walker, J.,
673 Walker, X.J., Walter, J.A., Waryszak, P., Weaver, R.J., Wedegärtner, R.E.M., Weller, D.L.,
674 Whelan, S., White, R.L., Wolfson, D.W., Wood, A., Yanco, S.W., Yen, J.D.L., Youngflesh, C.,
675 Zilio, G., Zimmer, C., Zimmerman, G.M. and Zitomer, R.A. (2023) 'Same data, different
676 analysts: variation in effect sizes due to analytical decisions in ecology and evolutionary
677 biology'. Available at:
678 https://ecoevovxiv.org/repository/view/6000/?utm_source=miragenews&utm_medium=miragenews&utm_campaign=news (Accessed: 1 August 2024).
679

680 Grimmett, L., Whitsed, R. and Horta, A. (2020) 'Presence-only species distribution models
681 are sensitive to sample prevalence: Evaluating models using spatial prediction stability
682 and accuracy metrics', *Ecological Modelling*, 431, p. 109194. Available at:
683 <https://doi.org/10.1016/j.ecolmodel.2020.109194>.

684 Hein, L., Bagstad, K.J., Obst, C., Edens, B., Schenau, S., Castillo, G., Soulard, F., Brown, C.,
685 Driver, A., Bordt, M., Steurer, A., Harris, R. and Caparrós, A. (2020) 'Progress in natural
686 capital accounting for ecosystems', *Science*, 367(6477), pp. 514–515. Available at:
687 <https://doi.org/10.1126/science.aaz8901>.

688 Herold, M., Mayaux, P., Woodcock, C.E., Baccini, A. and Schmullius, C. (2008) 'Some
689 challenges in global land cover mapping: An assessment of agreement and accuracy in
690 existing 1 km datasets', *Remote Sensing of Environment*, 112(5), pp. 2538–2556. Available
691 at: <https://doi.org/10.1016/j.rse.2007.11.013>.

692 Hijmans, R.J. (2023) 'terra: Spatial Data Analysis'. Available at: [https://CRAN.R-](https://CRAN.R-project.org/package=terra)
693 [project.org/package=terra](https://CRAN.R-project.org/package=terra).

694 Horvath, P., Halvorsen, R., Simensen, T. and Bryn, A. (2021) 'A comparison of three ways to
695 assemble wall-to-wall maps from distribution models of vegetation types', *GIScience &*

- 696 *Remote Sensing*, 58(8), pp. 1458–1476. Available at:
697 <https://doi.org/10.1080/15481603.2021.1996313>.
- 698 Jansen, J., Woolley, S.N.C., Dunstan, P.K., Foster, S.D., Hill, N.A., Haward, M. and Johnson,
699 C.R. (2022) ‘Stop ignoring map uncertainty in biodiversity science and conservation policy’,
700 *Nature Ecology & Evolution*, 6(7), pp. 828–829. Available at:
701 <https://doi.org/10.1038/s41559-022-01778-z>.
- 702 Keith, D.A., Ferrer-Paris, J.R., Ghoraba, S.M.M., Henriksen, S., Monyeke, M., Murray, N.J.,
703 Nicholson, E., Rowland, J.A., Skowno, A., Slingsby, J.A., Storeng, A.B., Valderrábano, M.
704 and Zager, I. (eds) (2024) *Guidelines for the application of IUCN Red List of ecosystems*
705 *categories and criteria version 2*. IUCN International Union for Conservation of Nature.
706 Available at: <https://doi.org/10.2305/IUCN.CH.2016.RLE.1.en>.
- 707 Keith, D.A., Ferrer-Paris, J.R., Nicholson, E., Bishop, M.J., Polidoro, B.A., Ramirez-Llodra,
708 E., Tozer, M.G., Nel, J.L., Mac Nally, R., Gregr, E.J., Watermeyer, K.E., Essl, F., Faber-
709 Langendoen, D., Franklin, J., Lehmann, C.E.R., Etter, A., Roux, D.J., Stark, J.S., Rowland,
710 J.A., Brummitt, N.A., Fernandez-Arcaya, U.C., Suthers, I.M., Wiser, S.K., Donohue, I.,
711 Jackson, L.J., Pennington, R.T., Iliffe, T.M., Gerovasileiou, V., Giller, P., Robson, B.J.,
712 Pettoirelli, N., Andrade, A., Lindgaard, A., Tahvanainen, T., Terauds, A., Chadwick, M.A.,
713 Murray, N.J., Moat, J., Pliscoff, P., Zager, I. and Kingsford, R.T. (2022) ‘A function-based
714 typology for Earth’s ecosystems’, *Nature*, 610(7932), pp. 513–518. Available at:
715 <https://doi.org/10.1038/s41586-022-05318-4>.
- 716 Keith, D.A., Ghoraba, S.M.M., Kaly, E., Jones, K.R., Oosthuizen, A., Obura, D., Costa, H.M.,
717 Daniels, F., Duarte, E., Grantham, H., Gudka, M., Norman, J., Shannon, L.J., Skowno, A.
718 and Ferrer-Paris, J.R. (2024) ‘Contributions of the IUCN Red List of Ecosystems to risk-
719 based design and management of protected and conserved areas in Africa’, *Conservation*
720 *Biology*, 38(3), p. e14169. Available at: <https://doi.org/10.1111/cobi.14169>.
- 721 Khatami, R., Mountrakis, G. and Stehman, S.V. (2016) ‘A meta-analysis of remote sensing
722 research on supervised pixel-based land-cover image classification processes: General
723 guidelines for practitioners and future research’, *Remote Sensing of Environment*, 177, pp.
724 89–100. Available at: <https://doi.org/10.1016/j.rse.2016.02.028>.
- 725 Kuhn, M. (2008) ‘Building Predictive Models in R Using the caret Package’, *Journal of*
726 *Statistical Software*, 28(5), pp. 1–26. Available at: <https://doi.org/10.18637/jss.v028.i05>.
- 727 Liddle, D.T. and Elliott, L.P. (2008) ‘Tiwi Island threatened plants 2006 to 2008: field survey,
728 population monitoring including establishment of a program to investigate the impact of
729 pigs, and weed control.’, p. 50.
- 730 Loosvelt, L., Peters, J., Skriver, H., Lievens, H., Van Coillie, F.M.B., De Baets, B. and
731 Verhoest, N.E.C. (2012) ‘Random Forests as a tool for estimating uncertainty at pixel-level

- 732 in SAR image classification’, *International Journal of Applied Earth Observation and*
733 *Geoinformation*, 19, pp. 173–184. Available at: <https://doi.org/10.1016/j.jag.2012.05.011>.
- 734 Maynard, J.J., Yeboah, E., Owusu, S., Buenemann, M., Neff, J.C. and Herrick, J.E. (2023)
735 ‘Accuracy of regional-to-global soil maps for on-farm decision-making: are soil maps
736 “good enough”?’ , *SOIL*, 9(1), pp. 277–300. Available at: [https://doi.org/10.5194/soil-9-277-](https://doi.org/10.5194/soil-9-277-2023)
737 2023.
- 738 McIver, D.K. and Friedl, M.A. (2001) ‘Estimating pixel-scale land cover classification
739 confidence using nonparametric machine learning methods’, *IEEE Transactions on*
740 *Geoscience and Remote Sensing*, 39(9), pp. 1959–1968. Available at:
741 <https://doi.org/10.1109/36.951086>.
- 742 Menkhorst, K.A. and Woinarski, J.C.Z. (1992) ‘Distribution of mammals in monsoon
743 rainforests of the Northern Territory’, *Wildlife Research*, 19, pp. 295–316. Available at:
744 <https://doi.org/10.1071/WR9920295>.
- 745 Mitchell, P.J., Downie, A.-L. and Diesing, M. (2018) ‘How good is my map? A tool for semi-
746 automated thematic mapping and spatially explicit confidence assessment’,
747 *Environmental Modelling & Software*, 108, pp. 111–122. Available at:
748 <https://doi.org/10.1016/j.envsoft.2018.07.014>.
- 749 Morales-Barquero, L., Lyons, M.B., Phinn, S.R. and Roelfsema, C.M. (2019) ‘Trends in
750 Remote Sensing Accuracy Assessment Approaches in the Context of Natural Resources’,
751 *Remote Sensing*, 11(19), p. 2305. Available at: <https://doi.org/10.3390/rs11192305>.
- 752 Mucina, L. (2019) ‘Biome: evolution of a crucial ecological and biogeographical concept’,
753 *New Phytologist*, 222(1), pp. 97–114. Available at: <https://doi.org/10.1111/nph.15609>.
- 754 Murray, N.J., Keith, D.A., Bland, L.M., Nicholson, E., Regan, T.J., Rodríguez, J.P. and
755 Bedward, M. (2017) ‘The use of range size to assess risks to biodiversity from stochastic
756 threats’, *Diversity and Distributions*, 23(5), pp. 474–483. Available at:
757 <https://doi.org/10.1111/ddi.12533>.
- 758 Murray, N.J., Keith, D.A., Duncan, A., Tizard, R., Ferrer-Paris, J.R., Worthington, T.A.,
759 Armstrong, K., Nyan Hlaing, Win Thuya Htut, Aung Htat Oo, Kyaw Zay Ya and Grantham, H.
760 (2020) ‘Myanmar’s terrestrial ecosystems: Status, threats and conservation opportunities’,
761 *Biological Conservation*, 252, p. 108834. Available at:
762 <https://doi.org/10.1016/j.biocon.2020.108834>.
- 763 Murray, N.J., Phinn, S.R., DeWitt, M., Ferrari, R., Johnston, R., Lyons, M.B., Clinton, N.,
764 Thau, D. and Fuller, R.A. (2019) ‘The global distribution and trajectory of tidal flats’, *Nature*,
765 565(7738), pp. 222–225. Available at: <https://doi.org/10.1038/s41586-018-0805-8>.
- 766 Naas, A.E., Halvorsen, R., Horvath, P., Wollan, A.K., Bratli, H., Brynildsrud, K., Finne, E.A.,
767 Keetz, L.T., Lieungh, E., Olson, C., Simensen, T., Skarpaas, O., Tandstad, H.R., Torma, M.,

- 768 Værland, E.S. and Bryn, A. (2023) 'What explains inconsistencies in field-based ecosystem
769 mapping?', *Applied Vegetation Science*, 26(1), p. e12715. Available at:
770 <https://doi.org/10.1111/avsc.12715>.
- 771 Naas, A.E., Keetz, L.T., Halvorsen, R., Horvath, P., Mienna, I.M., Simensen, T. and Bryn, A.
772 (2024) 'Choice of predictors and complexity for ecosystem distribution models: effects on
773 performance and transferability', *Ecography*, n/a(n/a), p. e07269. Available at:
774 <https://doi.org/10.1111/ecog.07269>.
- 775 Nagendra, H. and Rocchini, D. (2008) 'High resolution satellite imagery for tropical
776 biodiversity studies: the devil is in the detail', *Biodiversity and Conservation*, 17(14), pp.
777 3431–3442. Available at: <https://doi.org/10.1007/s10531-008-9479-0>.
- 778 Neave, G., Murphy, B.P., Tiwi Rangers, Andersen, A. and Davies, H.F. (2024) 'The intact and
779 the imperilled: contrasting mammal population trajectories between two large adjacent
780 islands', *Wildlife Research* [Preprint].
- 781 Nicholson, E., Andrade, A., Brooks, T.M., Driver, A., Ferrer-Paris, J.R., Grantham, H.S.,
782 Gudka, M.S., Keith, D.A., Kontula, T., Lindgaard, A., Londono-Murcia, M.C., Murray, N.J.,
783 Raunio, A., Rowland, J.A., Sievers, M., Skowno, A.L., Stevenson, S.L., Valderrabano, M.,
784 Vernon, C.M., Zager, I. and Obura, D. (2024) 'Roles of the Red List of Ecosystems in the
785 Kunming-Montreal Global Biodiversity Framework', *Nature Ecology & Evolution* [Preprint].
786 Available at: <https://doi.org/10.1038/s41559-023-02320-5>.
- 787 Noh, J.K., Echeverria, C., Kleemann, J., Koo, H., Fürst, C. and Cuenca, P. (2020) 'Warning
788 about conservation status of forest ecosystems in tropical Andes: National assessment
789 based on IUCN criteria', *PLOS ONE*. Edited by R. Nóbrega, 15(8), p. e0237877. Available at:
790 <https://doi.org/10.1371/journal.pone.0237877>.
- 791 Olofsson, P., Arévalo, P., Espejo, A.B., Green, C., Lindquist, E., McRoberts, R.E. and Sanz,
792 M.J. (2020) 'Mitigating the effects of omission errors on area and area change estimates',
793 *Remote Sensing of Environment*, 236, p. 111492. Available at:
794 <https://doi.org/10.1016/j.rse.2019.111492>.
- 795 Olson, D.M., Dinerstein, E., Wikramanayake, E.D., Burgess, N.D., Powell, G.V.N.,
796 Underwood, E.C., D'amico, J.A., Itoua, I., Strand, H.E., Morrison, J.C., Loucks, C.J., Allnutt,
797 T.F., Ricketts, T.H., Kura, Y., Lamoreux, J.F., Wettengel, W.W., Hedao, P. and Kassem, K.R.
798 (2001) 'Terrestrial Ecoregions of the World: A New Map of Life on Earth: A new global map
799 of terrestrial ecoregions provides an innovative tool for conserving biodiversity',
800 *BioScience*, 51(11), pp. 933–938. Available at: [https://doi.org/10.1641/0006-3568\(2001\)051\[0933:TEOTWA\]2.0.CO;2](https://doi.org/10.1641/0006-3568(2001)051[0933:TEOTWA]2.0.CO;2).
- 802 Pettorelli, N., Laurance, W.F., O'Brien, T.G., Wegmann, M., Nagendra, H. and Turner, W.
803 (2014) 'Satellite remote sensing for applied ecologists: opportunities and challenges',

804 *Journal of Applied Ecology*. Edited by E.J. Milner-Gulland, 51(4), pp. 839–848. Available at:
805 <https://doi.org/10.1111/1365-2664.12261>.

806 Pettorelli, N., Williams, J., Schulte to Bühne, H. and Crowson, M. (2024) ‘Deep learning and
807 satellite remote sensing for biodiversity monitoring and conservation’, *Remote Sensing in*
808 *Ecology and Conservation* [Preprint]. Available at: <https://doi.org/10.1002/rse2.415>.

809 Pontius Jr, R.G. and Millones, M. (2011) ‘Death to Kappa: birth of quantity disagreement
810 and allocation disagreement for accuracy assessment’, *International Journal of Remote*
811 *Sensing*, 32(15), pp. 4407–4429. Available at:
812 <https://doi.org/10.1080/01431161.2011.552923>.

813 QGIS Development Team (2018) ‘QGIS Geographic Information System’.

814 R Core Team (2018) ‘R: A language and environment for statistical computing’. Vienna,
815 Austria: R Foundation for Statistical Computing.

816 Regan, H.M., Colyvan, M. and Burgman, M.A. (2002) ‘A taxonomy and treatment of
817 uncertainty for ecology and conservation biology’, *Ecological Applications*, 12(2), pp. 618–
818 628. Available at: [https://doi.org/10.1890/1051-0761\(2002\)012\[0618:ATATOU\]2.0.CO;2](https://doi.org/10.1890/1051-0761(2002)012[0618:ATATOU]2.0.CO;2).

819 Remmel, T.K. (2009) ‘Investigating Global and Local Categorical Map Configuration
820 Comparisons Based on Coincidence Matrices’, *Geographical Analysis*, 41(2), pp. 144–157.
821 Available at: <https://doi.org/10.1111/j.1538-4632.2009.00738.x>.

822 Richards, A.E., Andersen, A.N., Schatz, J., Eager, R., Dawes, T.Z., Hadden, K., Scheepers,
823 K. and Van Der Geest, M. (2012) ‘Savanna burning, greenhouse gas emissions and
824 indigenous livelihoods: Introducing the Tiwi Carbon Study: THE TIWI CARBON STUDY’,
825 *Austral Ecology*, 37(6), pp. 712–723. Available at: <https://doi.org/10.1111/j.1442-9993.2012.02395.x>.

827 Rivas, C.A., Guerrero-Casado, J. and Navarro-Cerillo, R.M. (2021) ‘Deforestation and
828 fragmentation trends of seasonal dry tropical forest in Ecuador: impact on conservation’,
829 *Forest Ecosystems*, 8(1), p. 46. Available at: <https://doi.org/10.1186/s40663-021-00329-5>.

830 Rocchini, D., Foody, G.M., Nagendra, H., Ricotta, C., Anand, M., He, K.S., Amici, V.,
831 Kleinschmit, B., Förster, M., Schmidtlein, S., Feilhauer, H., Ghisla, A., Metz, M. and Neteler,
832 M. (2013) ‘Uncertainty in ecosystem mapping by remote sensing’, *Computers &*
833 *Geosciences*, 50, pp. 128–135. Available at: <https://doi.org/10.1016/j.cageo.2012.05.022>.

834 Rossiter, D.G., Poggio, L., Beaudette, D. and Libohova, Z. (2022) ‘How well does digital soil
835 mapping represent soil geography? An investigation from the USA’, *SOIL*, 8(2), pp. 559–
836 586. Available at: <https://doi.org/10.5194/soil-8-559-2022>.

837 RStudio Team (2020) ‘RStudio: Integrated Development for R’. Boston, MA: RStudio, PBC.
838 Available at: <http://www.rstudio.com>.

- 839 Russell-Smith, J. (1991) 'Classification, species richness, and environmental relations of
840 monsoon rain forest in northern Australia', *Journal of Vegetation Science*, 2(2), pp. 259–
841 278. Available at: <https://doi.org/10.2307/3235959>.
- 842 Scarth, P., Armston, J., Lucas, R. and Bunting, P. (2023) 'Vegetation Height and Structure -
843 Derived from ALOS-1 PALSAR, Landsat and ICESat/GLAS, Australia Coverage.' Available
844 at: <https://portal.tern.org.au/metadata/TERN/de1c2fef-b129-485e-9042-8b22ee616e66>.
- 845 Simensen, T., Horvath, P., Vollering, J., Erikstad, L., Halvorsen, R. and Bryn, A. (2020)
846 'Composite landscape predictors improve distribution models of ecosystem types',
847 *Diversity and Distributions*, 26(8), pp. 928–943. Available at:
848 <https://doi.org/10.1111/ddi.13060>.
- 849 Smith, A., Murphy, S., Herderson, D. and Erickson, K. (2023) 'Including imprecisely
850 georeferenced specimens improves accuracy of species distribution models and
851 estimates of niche breadth', *Global Ecology & Biogeography*, 32(3), pp. 342–355. Available
852 at: <https://doi.org/doi:10.1111/geb.13628>.
- 853 Stehman, S.V. (2009) 'Sampling designs for accuracy assessment of land cover',
854 *International Journal of Remote Sensing*, 30(20), pp. 5243–5272. Available at:
855 <https://doi.org/10.1080/01431160903131000>.
- 856 Stehman, S.V. and Foody, G.M. (2019) 'Key issues in rigorous accuracy assessment of land
857 cover products', *Remote Sensing of Environment*, 231, p. 111199. Available at:
858 <https://doi.org/10.1016/j.rse.2019.05.018>.
- 859 Trouvé, R., Jiang, R., Fedrigo, M., White, M.D., Kasel, S., Baker, P.J. and Nitschke, C.R.
860 (2023) 'Combining Environmental, Multispectral, and LiDAR Data Improves Forest Type
861 Classification: A Case Study on Mapping Cool Temperate Rainforests and Mixed Forests',
862 *Remote Sensing*, 15(1), p. 60. Available at: <https://doi.org/10.3390/rs15010060>.
- 863 UNSD (2021) *System of Environmental-Economic Accounting—Ecosystem Accounting:*
864 *Final Draft version 5*. Department of Economic and Social Affairs, Statistical Division,
865 United Nations, pp. 1–350. Available at:
866 https://unstats.un.org/unsd/envaccounting/seeaRev/SEEA_CF_Final_en.pdf (Accessed:
867 24 January 2024).
- 868 Venter, Z.S., Barton, D.N., Chakraborty, T., Simensen, T. and Singh, G. (2022) 'Global 10 m
869 Land Use Land Cover Datasets: A Comparison of Dynamic World, World Cover and Esri
870 Land Cover', *Remote Sensing*, 14(16), p. 4101. Available at:
871 <https://doi.org/10.3390/rs14164101>.
- 872 Venter, Z.S., Czúcz, B., Stange, E., Nowell, M.S., Simensen, T., Immerzeel, B. and Barton,
873 D.N. (2024) "Uncertainty audit" for ecosystem accounting: Satellite-based ecosystem
874 extent is biased without design-based area estimation and accuracy assessment',

- 875 *Ecosystem Services*, 66, p. 101599. Available at:
876 <https://doi.org/10.1016/j.ecoser.2024.101599>.
- 877 Viscarra Rossel, R.A., Chen, C., Grundy, M.J., Searle, R., Clifford, D. and Campbell, P.H.
878 (2015) 'The Australian three-dimensional soil grid: Australia's contribution to the
879 GlobalSoilMap project', *Soil Research*, 53(8), p. 845. Available at:
880 <https://doi.org/10.1071/SR14366>.
- 881 Watson, J.E.M., Keith, D.A., Strassburg, B.B.N., Venter, O., Williams, B. and Nicholson, E.
882 (2020) 'Set a global target for ecosystems', *Nature*, 578(7795), pp. 360–362. Available at:
883 <https://doi.org/10.1038/d41586-020-00446-1>.
- 884 Watson, J.E.M., Venegas-Li, R., Grantham, H., Dudley, N., Stolton, S., Rao, M., Woodley, S.,
885 Hockings, M., Burkart, K., Simmonds, J.S., Sonter, L.J., Sreekar, R., Possingham, H.P. and
886 Ward, M. (2023) 'Priorities for protected area expansion so nations can meet their
887 Kunming-Montreal Global Biodiversity Framework commitments', *Integrative
888 Conservation*, 2(3), pp. 140–155. Available at: <https://doi.org/10.1002/inc3.24>.
- 889 Whittaker, R.H. (1956) 'Vegetation of the Great Smoky Mountains', *Ecological Monographs*,
890 26(1), pp. 2–80. Available at: <https://doi.org/10.2307/1943577>.
- 891 Wilson, B.A. and Fensham, R.J. (1994) 'A comparison of classification systems for the
892 conservation of sparsely wooded plains on Melville Island, Northern Australia', *Australian
893 Geographer*, 25(1), pp. 18–31. Available at: <https://doi.org/10.1080/00049189408703095>.
- 894 Wohlfart, C., Wegmann, M. and Leimgruber, P. (2014) 'Mapping Threatened Dry Deciduous
895 Dipterocarp Forest in South-East Asia for Conservation Management', *Tropical
896 Conservation Science*, 7(4), pp. 597–613. Available at:
897 <https://doi.org/10.1177/194008291400700402>.
- 898 Wright, M.N. and Ziegler, A. (2017) 'Ranger: a fast implementation of random forests for
899 high dimensional data in C++ and R.', *Journal of Statistical Software*, 77(1), pp. 1–17.
900 Available at: <https://doi.org/doi:10.18637/jss.v077.i01>.
- 901 Wulder, M.A., Masek, J.G., Cohen, W.B., Loveland, T.R. and Woodcock, C.E. (2012)
902 'Opening the archive: How free data has enabled the science and monitoring promise of
903 Landsat', *Remote Sensing of Environment*, 122, pp. 2–10. Available at:
904 <https://doi.org/10.1016/j.rse.2012.01.010>.
- 905 Xiao, H., Driver, A., Etter, A., Keith, D.A., Obst, C., Traurig, M.J. and Nicholson, E. (2024)
906 'Synergies and complementarities between ecosystem accounting and the Red List of
907 Ecosystems', *Nature Ecology & Evolution*, 8, pp. 1794–1803. Available at:
908 <https://doi.org/10.1038/s41559-024-02494-6>.
- 909 Young, A.R., Davies, H.F., Ayre, M.L., Brekelmans, A., Bryan, B.A., Elith, J., Hadden, K.,
910 Kerinaiua, M., Keith, D.A., Lewis, D.L., Munkara-Murray, K.M., Ryan, S., Spencer, M. and

911 Nicholson, E. (2024) 'Applying the Global Ecosystem Typology to classify, describe, and
912 map ecosystems from regional data and Indigenous knowledge'. EcoEvoRxiv. Available at:
913 <https://doi.org/10.32942/X20P75>.

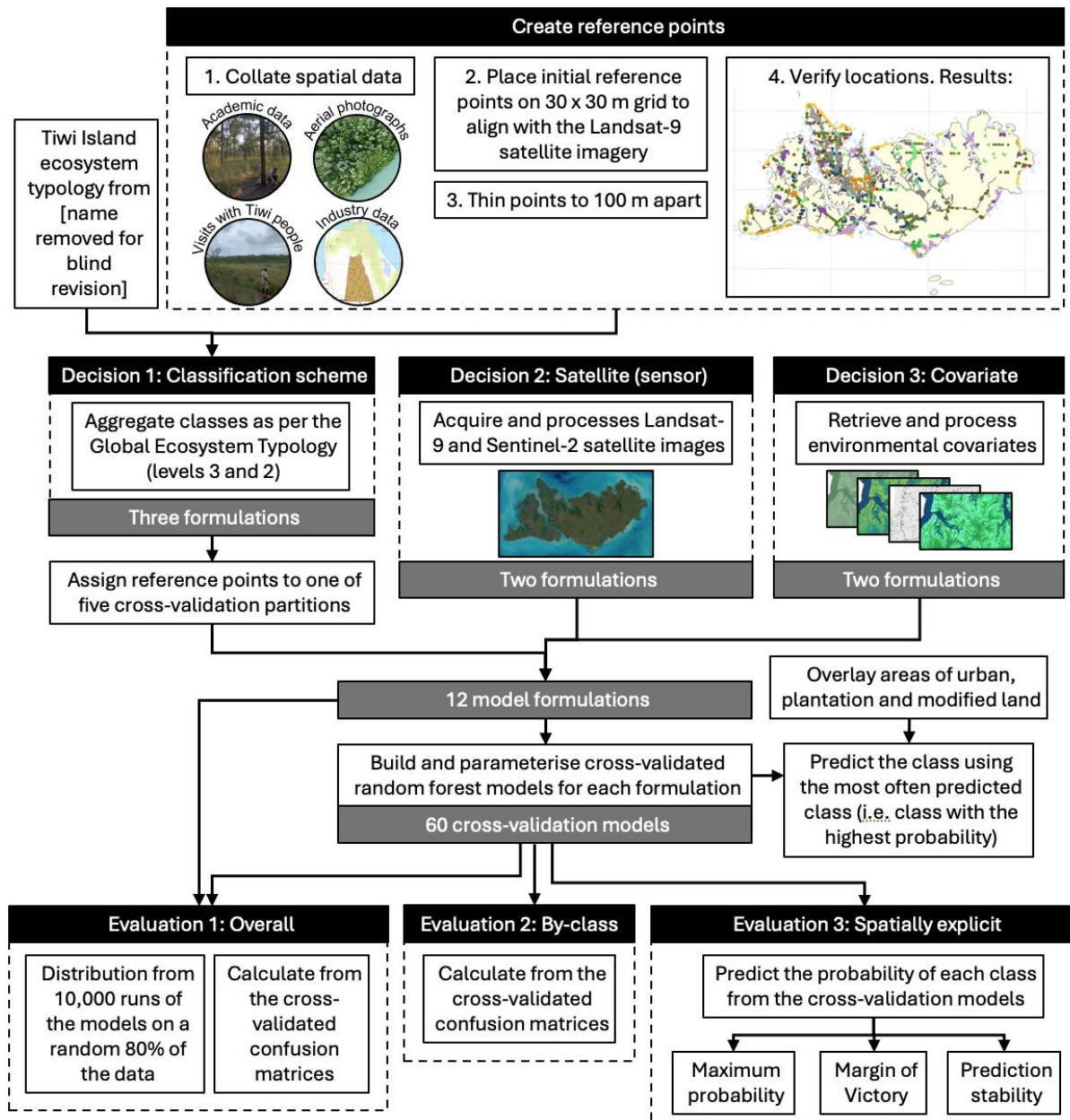
914 Yu, Le, Liang, L., Wang, J., Zhao, Y., Cheng, Q., Hu, L., Liu, S., Yu, Liang, Wang, X., Zhu, P.,
915 Li, Xueyan, Xu, Y., Li, C., Fu, W., Li, Xuecao, Li, W., Liu, C., Cong, N., Zhang, H., Sun, F., Bi,
916 X., Xin, Q., Li, D., Yan, D., Zhu, Z., Goodchild, M.F. and Gong, P. (2014) 'Meta-discoveries
917 from a synthesis of satellite-based land-cover mapping research', *International Journal of*
918 *Remote Sensing*, 35(13), pp. 4573–4588. Available at:
919 <https://doi.org/10.1080/01431161.2014.930206>.

920

921

922 **Supplementary material**

923 **Appendix 1 – Modelling methodology**



924 Figure 5. Flow chart of the methods to test three modelling decisions on mapping the
 925 extent of ecosystems and assess the decisions with three assessment metrics.
 926

927 **Appendix 2 – Software**

928 **Software**

929 QGIS (version 3.22.12)

930 Google Earth Engine (Gorelick et al., 2017)

931 R (version 4.3.0) (R Core Team, 2018)
 932 R-studio (version 2023.09.1+949) (RStudio Team, 2020)

933 **R packages**

934 Satellite imagery and environmental covariates:
 935 ‘rgee’ (version 1.1.6.9999) (Aybar *et al.*, 2020)
 936 ‘rgeeExtra’ (version 0.0.1) (Aybar *et al.*, 2020)

937 Data cleaning and manipulation:
 938 ‘enmSdmX’ package (version 1.1.2) (Smith *et al.*, 2023)
 939 ‘dplyr’ (version 1.1.2) (Wickham *et al.*, 2023)
 940 ‘tidyr’ (version 1.3.0) (Wickham, Vaughan and Girlich, 2023)
 941 ‘stringr’ (version 1.5.0) (Wickham, 2022)

942 Spatial data handling:
 943 ‘sf’ (version 1.0-16) (Pebesma, 2018)
 944 ‘terra’ (version 1.7-29) (Hijmans, 2023)

945 Model fitting, evaluation and prediction:
 946 ‘ranger’ (version 0.15.1) (Wright and Ziegler, 2017)
 947 ‘vip’ (version 0.3.2) (Greenwell and Boehmke, 2020)
 948 ‘caret’ (version 6.0-94) (Kuhn, 2008)

949 Visualisations:
 950 ‘tidyterra’ (version 0.4.0) (Hernangomez, 2024)
 951 ‘ggplot2’ (version 3.4.3) (Wickham, 2016)
 952 ‘ggspatial’ (version 1.1.8) (Dunnington, 2023)
 953 ‘ggh4x’ (version 0.2.8) (van den Brand, 2024)
 954 ‘ggnewscale’ (version 0.4.9) (Campitelli, 2023)
 955 ‘ggstance’ (version 0.3.7) (Henry, Wickham and Chang, 2024)

956 **Appendix 3 – Satellite imager processing**

957 We applied scaling factors to the satellite images obtained from the Landsat-9 satellite
 958 with the OLI-2 sensor and from the Sentinel-2 satellite with the MSI sensor. For the optical
 959 bands (i.e. the name begins with SR) of Landsat-9 OLI images, the band was first multiplied
 960 by 2.75×10^{-5} then minuses 0.2. For the thermal bands (i.e. the name begins with ST) of
 961 Landsat-9, the band was first multiplied by 3.41802×10^{-3} then added 149. The Sentinel-2
 962 images were scaled by 0.0001 to reverse the scaling factor applied for efficient data
 963 storage.

964
 965 To mask the clouds in the Landsat-9 images, we used the quality assessment bands for the
 966 cloud and cloud shadow (bits 3 and 5). For the Sentinel-2 images, we used the Scene
 967 Classification Layer and removed the pixels classified as no data (SCL = 0), saturated (SCL
 968 = 1), medium or high cloud probability (SCL = 8 and 9), high cirrus cloud (SCL = 10), snow
 969 and ice (SCL = 11).

970 **Appendix 4 – Environmental covariates**

971 We tested correlation in the variables using the absolute value of the Pearson’s correlation
972 coefficient with a cut-off of 0.7 (Figure 2). The red, green and blue bands were all highly
973 correlated. NDVI was least correlated to the red band for both satellites.

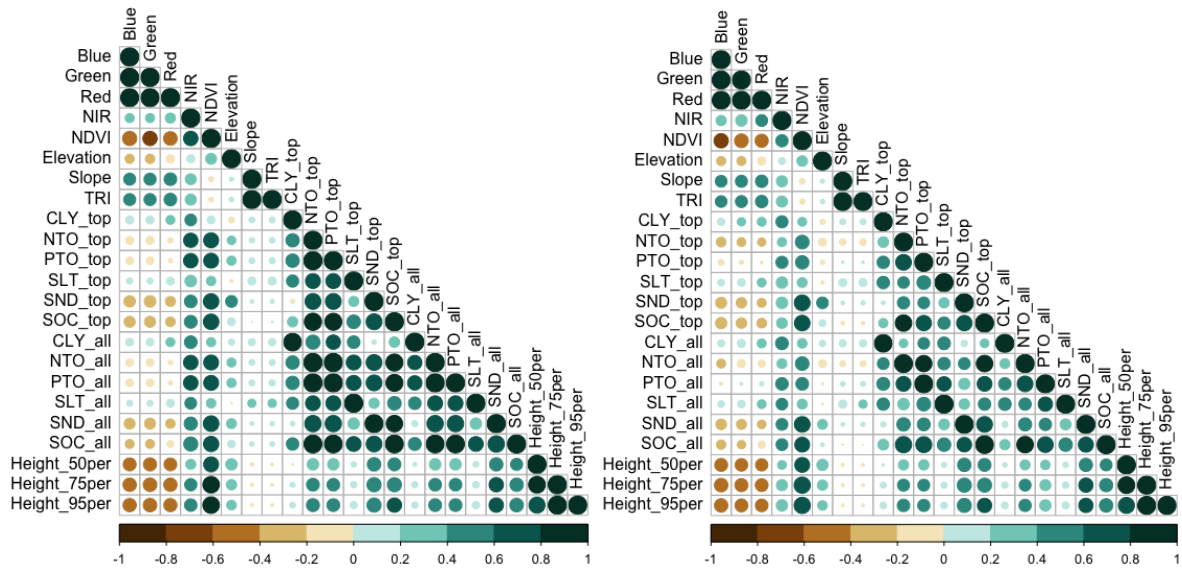
974 Each of the soil variables were correlated between the two depths. We retained the top 30
975 cm variables to reflect the root zone of more of the plant species. Nitrogen, phosphorus
976 and soil sand content were highly correlated to near infrared and NDVI for the Landsat-9
977 variables and hence removed. We retained slope instead of the correlated TRI to represent
978 rainfall run-off and easier interpretation of the results. Each of the vegetation biomass
979 height variables were correlated. We retained the height of 50% of the biomass as it was
980 least correlated to all the other covariates.

981

982 Table 2. Details of the environmental covariates.

Layer	Description	Rational	Source
<i>Satellite image covariates</i>			
Red Green Blue NIR	The red, green, blue and near infrared bands.	Spectral characteristics represent physical and chemical attributes of the ecosystem.	Landsat-9 satellite atmospherically corrected surface reflectance (level 2, collection 2, tier 1) courtesy of the United States Geological Survey (USGS). For Landsat-9, the red band is B4, green is B3, blue is B2 and near infrared is B5. Sentinel-2 surface reflectance harmonised collection (level-2A) with atmospheric correction from the Copernicus Sentinel missions are by the European Space Agency (ESA). For Sentinel-2, the red band is B4, green is B3, blue is B2 and near infrared is B8.
NDVI	Normalised difference vegetation index.	Greenness of the canopy which is correlated to primary productivity.	Calculated from the satellite image using the red and near infrared bands where: $NDVI = \frac{NIR - Red}{NIR + Red}$
<i>Additional covariates</i>			
Height_50 Height_75 Height_95	The height where 50, 75 and 95% of the plant cover has been intercepted.	The height of the vegetation biomass relates to the vegetation structure.	Terrestrial Ecosystem Research Network https://portal.tern.org.au/metadata/TERN/de1c2fef-b129-485e-9042-8b22ee616e66
Elev	Elevation in meters.	The elevation is a proxy for range of environmental relationships including access to groundwater, influence of floods, exposure to wind on hilltops, and exposure to wave disturbances on coastal ecosystem.	The Smoothed Digital Elevation model (DEM-S) at a 5 m resolution from the Shuttle Radar Topography Mission (SRTM) by from Geoscience Australia in 2000 https://developers.google.com/earth-engine/datasets/catalog/AU_GA_DEM_1SEC_v10_DEM-S
Slp TRI	Slope in degrees. Topographic roughness index.	The topographic measures of the slope, position and roughness also relate to soil moisture and run off which strongly drive ecosystem functioning.	Created using the 'terrain' function from the 'terra' package in R on the elevation model. Slope was computed with the four neighbouring cells and measured in degrees.
Clay Silt Sand SOC NTO PTO	Percentage of 1) clay, 2) silt, 3) sand, 4) soil organic carbon, 5) nitrogen or 6) phosphorus in the top 30 cm and 2 m of the soil.	The soil composition influences many aspects of plant growth and soil moisture, including nutrient availability and drainage.	Soil and Landscape Grid of Australia. Averaged by the depth over which the attribute was measured (depth-weighted average). https://dx.doi.org/10.1071/SR14366

983



984
 985 Figure 6. Correlation of the environmental predictors at a 30 m resolution with Landsat-9
 986 satellite imagery using the OLI-2 sensor (left) and a 10 m resolution with Sentinel-2 satellite
 987 imagery using the MSI sensor (right).

988 **Appendix 5 – Model evaluation**

989 For the confusion matrix

		Reference	
		1	0
Predicted	1	a	b
	0	c	d

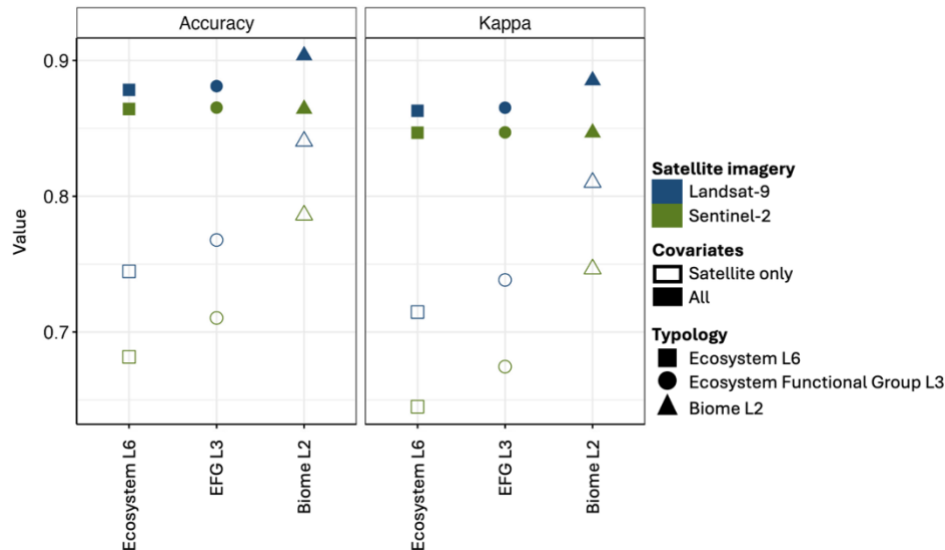
990 a represents the number of true positive values, b the false positives, c the false negatives
 991 and d the true negatives. This confusion matrix is used to calculate the evaluation metrics
 992 in Table 3.

993

994 Table 3. Descriptions of the overall and by-class evaluation metrics.

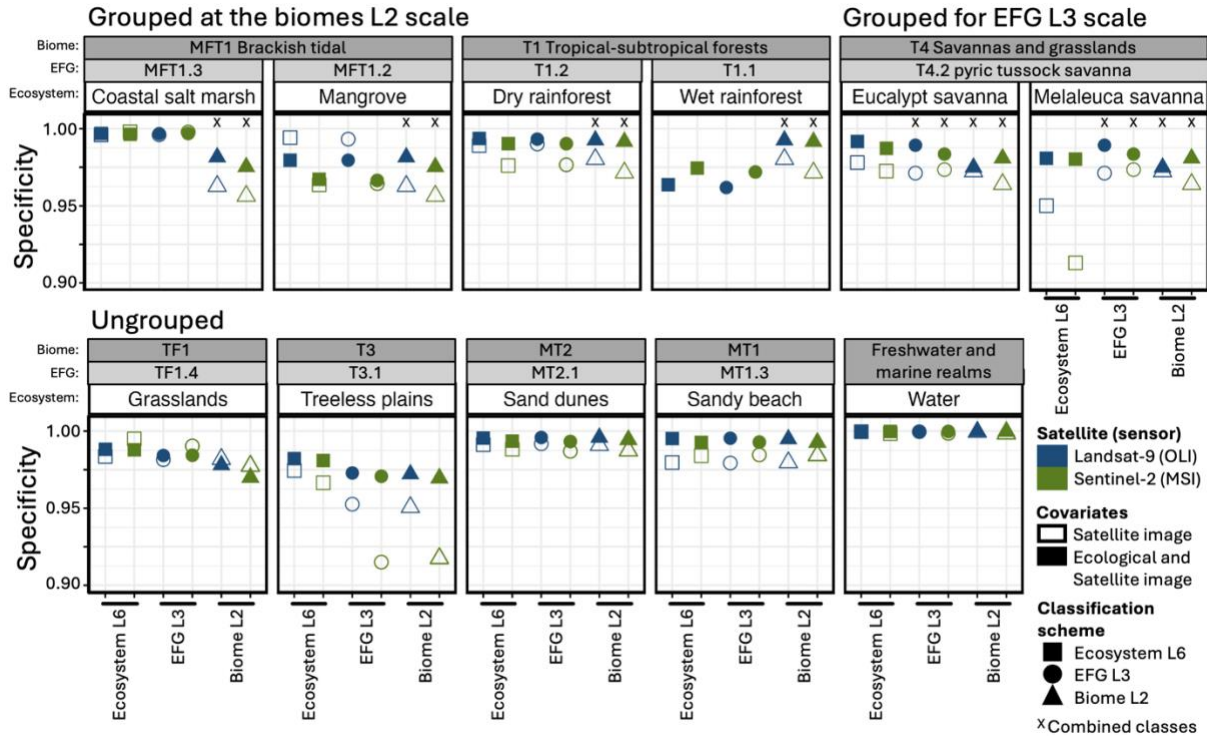
Evaluation metric	Other names	Equation	Description
<i>Overall metrics</i>			
Accuracy		$\frac{a + d}{a + b + c + d}$	A measure of agreement between the predicted and true values, such that 1 indicates perfect agreements and 0 indicates no agreement.
Kappa statistic	Cohen's kappa	$N = a + b + c + d$ $p_0 = \text{Accuracy}$ $p_e = \frac{a + c}{N} \times \frac{a + b}{N} + \frac{b + d}{N} \times \frac{c + d}{N}$ $Kappa = \frac{p_0 - p_e}{1 - p_e}$	A measure of agreement between the predicted and true values, such that 1 indicates perfect agreements and 0 indicates no more agreement than expected by chance.
Out-of-bag error (OOB)	Out-of-bag score		The average error for the random forest trees using bootstrap aggregation and calculated on the out-of-bag samples.
<i>By-class metrics</i>			
Sensitivity	Producer's accuracy, recall, true positive rate	$\frac{a}{a + c}$	The ability of the model to correctly identify all the true cases from those known to be true.
Specificity	True negative rate	$\frac{d}{b + d}$	The ability of the model to correctly identify all the false cases from those known to be false.
Precision	User's accuracy, positive predicted value	$\frac{a}{a + b}$	The ability of the model to correctly identify all the true cases from those predicted to the class.
F1		$2 \times \frac{\text{Sensitivity} \times \text{Precision}}{\text{Sensitivity} + \text{Precision}}$	A balance of the models ability to predict the true cases from those known to be true (i.e. sensitivity) and the correctly true from all those predicted to be true (i.e. precision).
Negative predicted value		$\frac{d}{c + d}$	The ability of the model to correctly identify all the false cases from those predicted to be false.

995 **Appendix 6 – Additional model results**

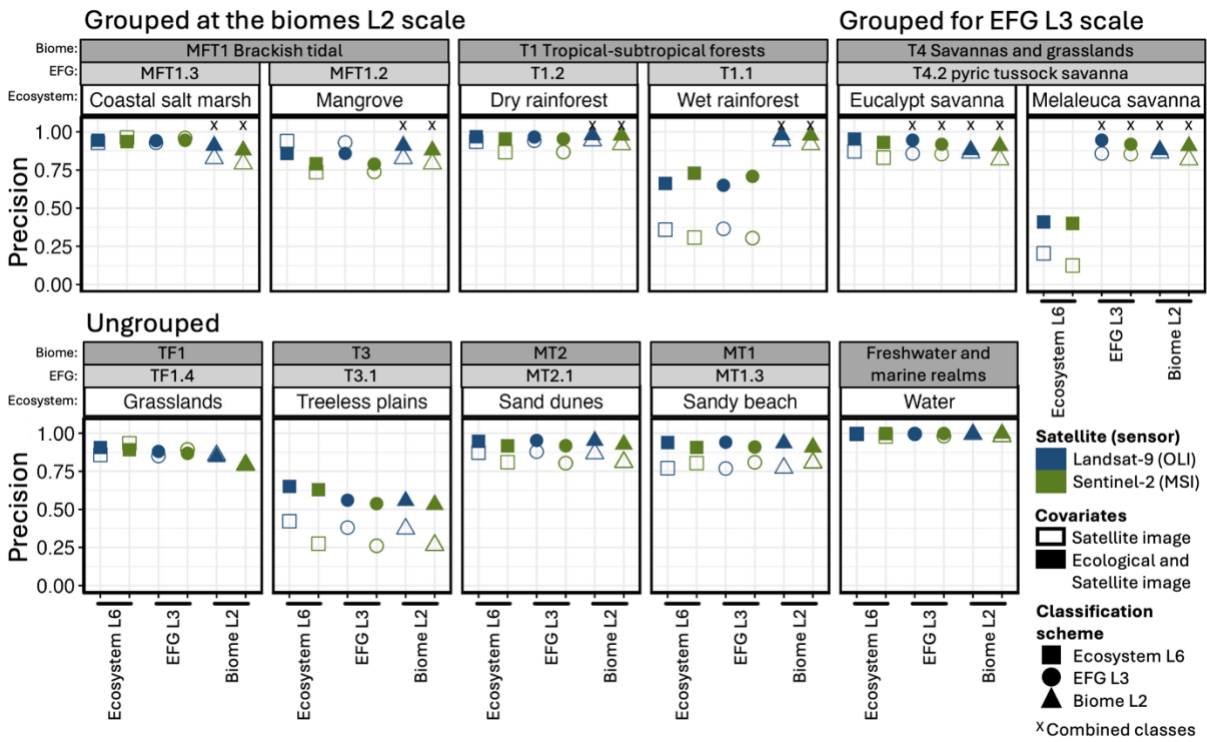


996
 997 Figure 7. The mean accuracy and kappa statistics calculated from the confusion matrix of
 998 12 model formulations varying at three modelling decisions and each run with five cross-
 999 validated models. The modelling decisions were the typology (shape), covariates (fill) and
 1000 satellite imagery (colours).

1001 A)

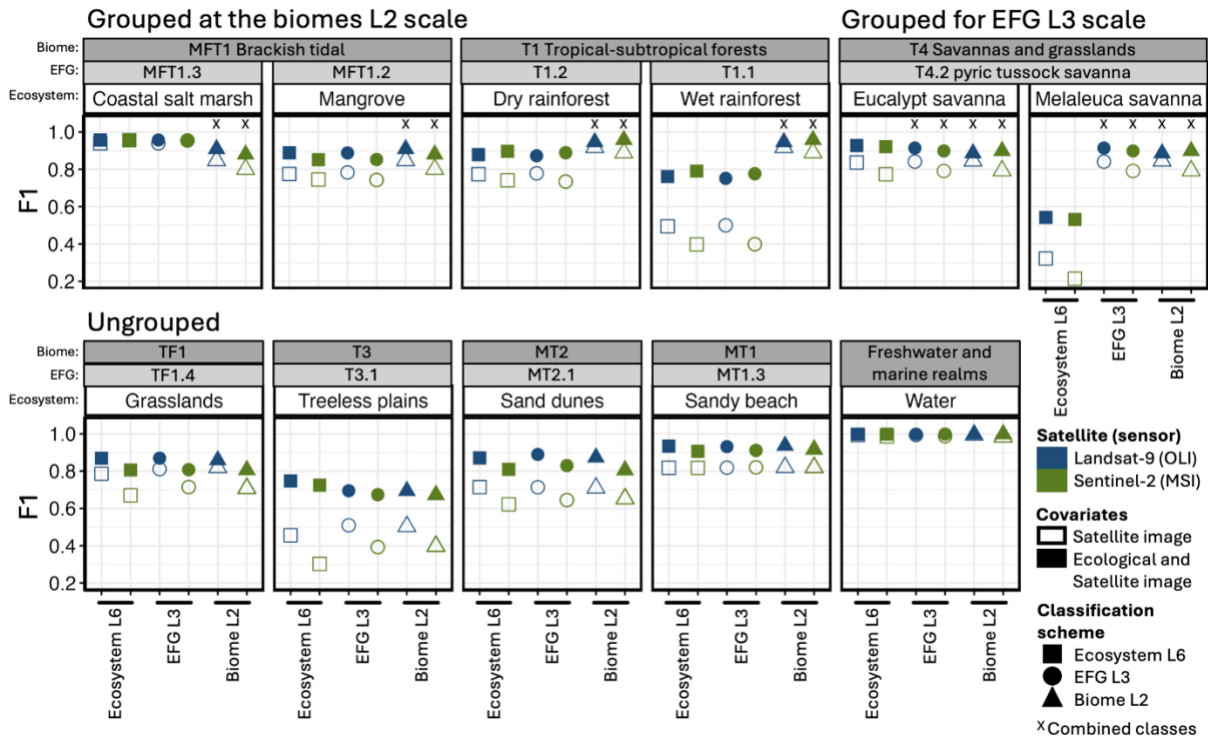


1002
1003 B)

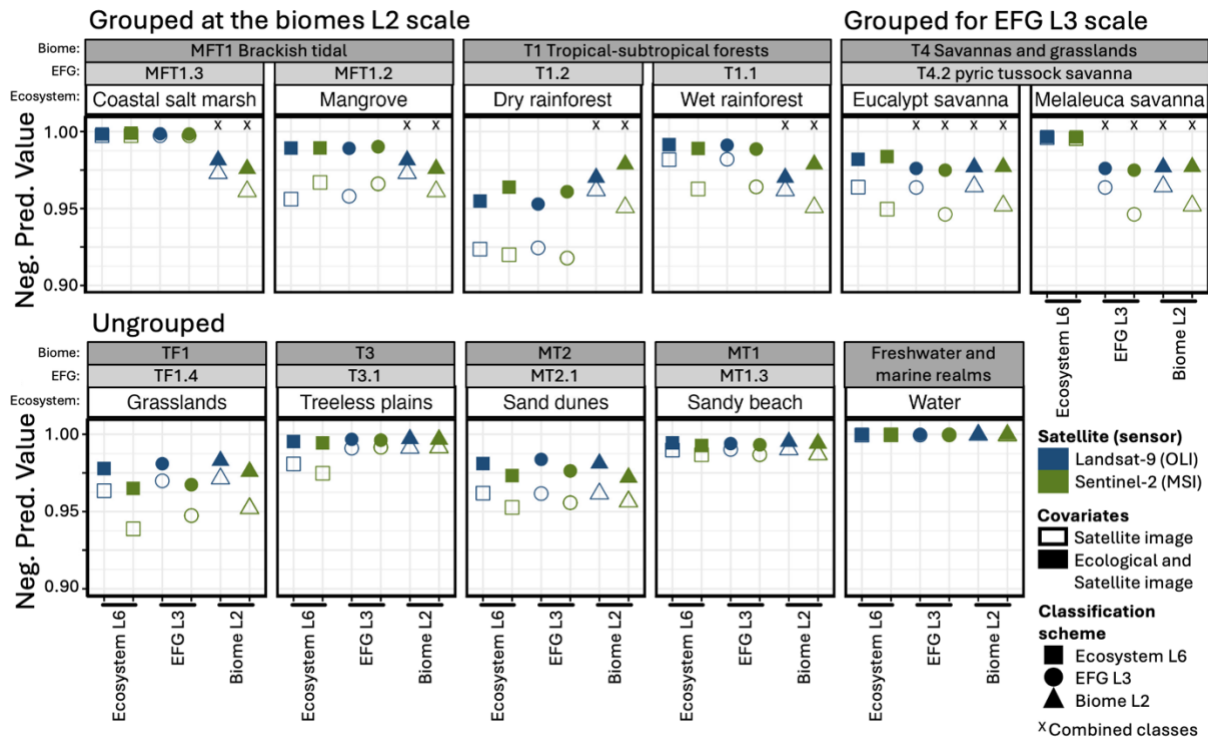


1004

1005 C)

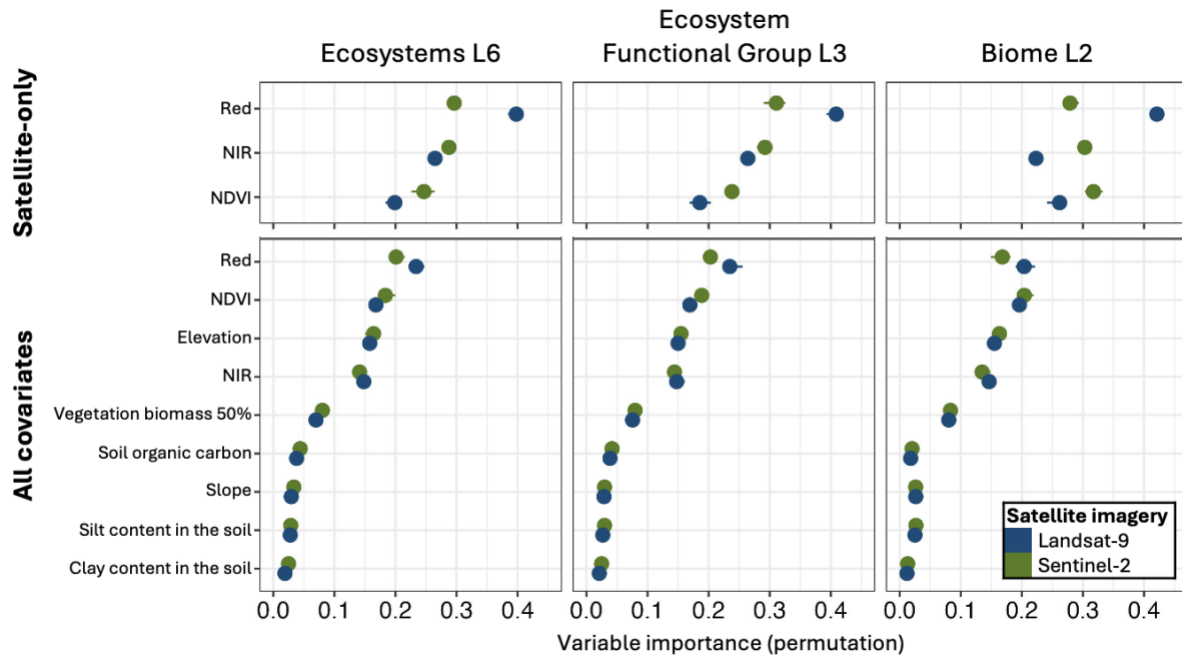


1006
1007 D)



1008

1009 Figure 8. The four by-class evaluation metrics specificity (A), precision (B), F1 (C), and
 1010 negative predicted value (D) measured for three classification schemes (shape), two
 1011 satellite/sensors (colour) and two covariate sets (fill). When multiple ecosystems (shape:
 1012 square, label above: white) were aggregated into an ecosystem functional group (shape:
 1013 circle, label: light grey) or into a biome (shape: triangle, label: dark grey), the class is
 1014 indicated by an x.



1015 Figure 9. Importance of the environmental covariates in the ecosystem classification
 1016 model across three classification schemes (columns), two options for the covariates (row)
 1017 and two satellite (colours). NDVI is for the normalised difference vegetation index and NIR
 1018 is for the near-infrared band from the satellite image.
 1019

1020 **Appendix 7 – confusion matrices**

1021 Table 4. Confusion matrix for the ecosystem classification model using Landsat-9 satellite
 1022 imagery from the OLI-2 sensor as the only covariates.

	Training points											Total	UA	CE	
	Coastal salt marsh	Dry rainforest	Eucalypt savanna	Grassland and sedgeland	Mangrove	Melaleuca savanna	Treeless plains	Sand dunes	Sandy beach	Water	Wet rainforest				
Predicted type															
Coastal salt marsh	285	0	0	4	1	0	0	1	13	3	0	307	0.93	0.07	
Dry rainforest	0	754	0	0	2	0	0	0	0	0	50	806	0.94	0.06	
Eucalypt savanna	0	7	745	42	9	9	20	14	0	0	8	854	0.87	0.13	
Grassland and sedgeland	7	0	13	511	43	1	4	2	0	0	15	596	0.86	0.14	
Mangrove	0	3	0	10	461	0	0	0	0	0	17	491	0.94	0.06	
Melaleuca savanna	0	1	111	76	0	74	79	22	0	0	0	363	0.20	0.80	
Treeless plains	0	1	39	26	0	12	106	67	0	0	0	251	0.42	0.58	
Sand dunes	1	0	0	0	0	0	5	321	41	0	0	368	0.87	0.13	
Sandy beach	7	0	0	0	0	0	0	104	373	0	0	484	0.77	0.23	
Water	0	0	0	1	0	0	0	0	1	411	0	413	1.00	0.00	
Wet rainforest	0	376	19	34	182	0	0	0	0	0	343	954	0.36	0.64	
Total	300	1142	927	704	698	96	214	531	428	414	433	5887			
PA	0.95	0.66	0.80	0.73	0.66	0.77	0.50	0.60	0.87	0.99	0.79				
OE	0.05	0.34	0.20	0.27	0.34	0.23	0.50	0.40	0.13	0.01	0.21				

Model formulation

Classification scheme: Ecosystem (level 6 of the Global Ecosystem typology)

Satellite/sensor: Landsat-9/OLI-2

Covariate set: Satellite image covariates only

PA: Producer's accuracy

UA: User's accuracy

OE: Omission error

CE: Commission error

1023

1024 Table 5. Confusion matrix for the ecosystem classification model using Landsat-9 satellite
 1025 imagery from the OLI-2 sensor and using satellite image and additional covariates.

Predicted type	Training points											Total	UA	CE
	Coastal salt marsh	Dry rainforest	Eucalypt savanna	Grassland and sedgeland	Mangrove	Melaleuca savanna	Treeless plains	Sand dunes	Sandy beach	Water	Wet rainforest			
Coastal salt marsh	291	0	0	8	1	0	0	1	7	0	0	308	0.94	0.06
Dry rainforest	0	919	0	0	6	0	0	0	0	0	24	949	0.97	0.03
Eucalypt savanna	0	3	837	18	5	1	1	5	0	0	8	878	0.95	0.05
Grassland and sedgeland	3	0	6	588	36	1	4	5	0	0	6	649	0.91	0.09
Mangrove	0	45	1	52	643	0	0	1	0	0	7	749	0.86	0.14
Melaleuca savanna	0	1	37	18	2	77	21	32	0	0	0	188	0.41	0.59
Treeless plains	0	0	27	19	0	17	188	38	0	0	0	289	0.65	0.35
Sand dunes	1	1	0	0	0	0	0	428	22	0	0	452	0.95	0.05
Sandy beach	5	0	0	0	0	0	0	21	398	0	0	424	0.94	0.06
Water	0	0	0	0	0	0	0	0	1	414	0	415	1.00	0.00
Wet rainforest	0	173	19	1	5	96	0	0	0	0	388	586	0.66	0.34
Total	300	1142	927	704	698	96	214	513	428	414	433	5887		
PA	0.97	0.80	0.90	0.84	0.92	0.80	0.88	0.81	0.93	1.00	0.9			
OE	0.03	0.20	0.10	0.16	0.08	0.20	0.12	0.19	0.07	0.00	0.1			

Model formulation

Classification scheme: Ecosystem (level 6 of the Global Ecosystem typology)

Satellite/sensor: Landsat-9/OLI-2

Covariate set: Satellite image and additional covariates

PA: Producer's accuracy

UA: User's accuracy

OE: Omission error

CE: Commission error

1027 Table 6. Confusion matrix for the ecosystem classification model using Sentinel-2 satellite
 1028 imagery from the MSI sensor as the only covariates.

Predicted type	Training points											Total	UA	CE
	Coastal salt marsh	Dry rainforest	Eucalypt savanna	Grassland and sedgeland	Mangrove	Melaleuca savanna	Treeless plains	Sand dunes	Sandy beach	Water	Wet rainforest			
Coastal salt marsh	285	0	0	3	1	0	0	1	5	1	0	296	0.96	0.04
Dry rainforest	0	739	0	2	17	0	0	1	0	0	93	852	0.87	0.13
Eucalypt savanna	0	2	671	45	16	16	23	12	0	0	22	807	0.83	0.17
Grassland and sedgeland	3	0	1	368	11	3	3	3	0	0	2	394	0.93	0.07
Mangrove	0	55	0	61	527	0	0	1	0	0	72	716	0.74	0.26
Melaleuca savanna	0	0	217	137	3	72	113	33	0	0	1	576	0.13	0.88
Treeless plains	0	0	19	31	0	5	72	131	4	0	0	262	0.27	0.73
Sand dunes	2	0	0	0	0	0	3	268	58	0	0	331	0.81	0.19
Sandy beach	7	0	0	0	0	0	0	79	356	1	0	443	0.80	0.20
Water	3	0	0	1	0	0	0	0	5	412	0	421	0.98	0.02
Wet rainforest	0	346	19	56	123	0	0	2	0	0	243	789	0.31	0.69
Total	300	1142	927	704	698	96	214	531	428	414	433	5887		
PA	0.95	0.65	0.72	0.52	0.76	0.75	0.34	0.5	0.83	1.00	0.56			
OE	0.05	0.35	0.28	0.48	0.24	0.25	0.66	0.5	0.17	0.00	0.44			

Model formulation

Classification scheme: Ecosystem (level 6 of the Global Ecosystem typology)

Satellite/sensor: Sentinel-2/MSI

Covariate set: Satellite image covariates only

PA: Producer's accuracy

UA: User's accuracy

OE: Omission error

CE: Commission error

1029

1030 Table 7 . Confusion matrix for the ecosystem classification model using Sentinel-2 satellite
 1031 imagery from the MSI sensor and using satellite image and additional covariates.

	Training points											Total	UA	CE
	Coastal salt marsh	Dry rainforest	Eucalypt savanna	Grassland and sedgeland	Mangrove	Melaleuca savanna	Treeless plains	Sand dunes	Sandy beach	Water	Wet rainforest			
Coastal salt marsh	294	0	0	7	1	0	0	5	7	0	0	314	0.94	0.06
Dry rainforest	0	966	1	1	16	0	0	1	0	0	27	1012	0.95	0.05
Eucalypt savanna	0	1	846	30	5	0	2	4	0	0	21	909	0.93	0.07
Grassland and sedgeland	1	1	4	518	26	3	6	19	1	0	2	581	0.89	0.11
Mangrove	0	51	1	107	644	0	0	3	0	0	8	814	0.79	0.21
Melaleuca savanna	0	0	34	21	2	76	21	35	0	0	1	190	0.40	0.60
Treeless plains	0	0	30	17	0	16	183	44	1	0	0	291	0.63	0.37
Sand dunes	0	0	1	2	0	0	2	385	30	0	0	420	0.92	0.08
Sandy beach	5	0	0	0	0	0	0	35	388	0	0	428	0.91	0.09
Water	0	0	0	0	0	0	0	0	1	414	0	415	1.00	0.00
Wet rainforest	0	123	10	1	4	1	0	0	0	0	374	513	0.73	0.27
Total	300	1142	927	704	698	96	214	531	428	414	433	5887		
PA	0.98	0.85	0.91	0.74	0.92	0.79	0.86	0.73	0.91	1.00	0.86			
OE	0.02	0.15	0.09	0.26	0.08	0.21	0.14	0.27	0.09	0.00	0.14			

Model formulation

Classification scheme: Ecosystem (level 6 of the Global Ecosystem typology)

Satellite/sensor: Sentinel-2/MSI

Covariate set: Satellite image and additional covariates

PA: Producer's accuracy

UA: User's accuracy

OE: Omission error

CE: Commission error

1032

1033 Table 8. Confusion matrix for the ecosystem functional group classification model using
 1034 Landsat-9 satellite imagery from the OLI-2 sensor as the only covariates.

	Training points										Total	UA	CE	
	Dry rainforest	Grassland and sedgeland	Mangrove	Coastal salt marsh	Sandy beach	Sand dunes	Savanna	Treeless plains	Water	Wet rainforest				
Predicted type														
Dry rainforest	758	0	2	0	0	0	0	0	0	0	45	805	0.94	0.06
Grassland and sedgeland	1	546	41	7	0	6	22	5	0	14	642	642	0.85	0.15
Mangrove	3	10	472	0	0	0	0	0	0	22	507	507	0.93	0.07
Coastal salt marsh	0	4	1	285	13	1	0	0	3	0	307	307	0.93	0.07
Sandy beach	0	0	0	7	375	106	0	0	0	0	488	488	0.77	0.23
Sand dunes	0	0	0	1	39	319	0	4	0	0	363	363	0.88	0.12
Savanna	7	60	9	0	0	16	845	40	0	8	985	985	0.86	0.14
Treeless plains	0	49	0	0	0	83	137	165	0	0	434	434	0.38	0.62
Water	0	1	0	0	1	0	0	0	411	0	413	413	1.00	0.00
Wet rainforest	373	34	173	0	0	0	19	0	0	344	943	943	0.36	0.64
Total	1142	704	698	300	428	531	1023	214	414	433	5887			
PA	0.66	0.78	0.68	0.95	0.88	0.60	0.83	0.77	0.99	0.79				
OE	0.34	0.22	0.32	0.05	0.12	0.40	0.17	0.23	0.01	0.21				

Model formulation

Classification scheme: Ecosystem Functional Group (level 3 of the Global Ecosystem typology)

Satellite/sensor: Landsat-9/OLI-2

Covariate set: Satellite image covariates only

PA: Producer's accuracy

UA: User's accuracy

OE: Omission error

CE: Commission error

1035

1036 Table 9. Confusion matrix for the ecosystem functional group classification model using
 1037 Landsat-9 satellite imagery from the OLI-2 sensor and using the satellite image and
 1038 additional covariates.

		Training points										Total	UA	CE
		Dry rainforest	Grassland and sedgeland	Mangrove	Coastal salt marsh	Sandy beach	Sand dunes	Savanna	Treeless plains	Water	Wet rainforest			
Predicted type	Dry rainforest	909	1	6	0	0	0	0	0	0	25	941	0.97	0.03
	Grassland and sedgeland	0	605	39	2	0	12	13	10	0	6	687	0.88	0.12
	Mangrove	46	50	642	0	0	1	1	0	0	8	748	0.86	0.14
	Coastal salt marsh	0	6	1	292	11	0	0	0	0	0	310	0.94	0.06
	Sandy beach	0	0	0	5	395	20	0	0	0	0	420	0.94	0.06
	Sand dunes	0	0	0	1	21	443	0	0	0	0	465	0.95	0.05
	Savanna	4	22	5	0	0	5	905	8	0	8	957	0.95	0.05
	Treeless plains	0	19	0	0	0	50	85	196	0	0	350	0.56	0.44
	Water	0	0	0	0	1	0	0	0	414	0	415	1	0
	Wet rainforest	183	1	5	0	0	0	19	0	0	386	594	0.65	0.35
	Total	1142	704	698	300	428	531	1023	214	414	433	5887		
PA	0.8	0.86	0.92	0.97	0.92	0.83	0.88	0.92	1	0.89				
OE	0.2	0.14	0.08	0.03	0.08	0.17	0.12	0.08	0	0.11				

Model formulation

Classification scheme: Ecosystem Functional Group (level 3 of the Global Ecosystem typology)

Satellite/sensor: Landsat-9/OLI-2

Covariate set: Satellite image and additional covariates

PA: Producer's accuracy

UA: User's accuracy

OE: Omission error

CE: Commission error

1039

1040 Table 10. Confusion matrix for the ecosystem functional group classification model using
 1041 Sentinel-2 satellite imagery from the MSI sensor as the only covariates.

	Training points										Total	UA	CE	
	Dry rainforest	Grassland and sedgeland	Mangrove	Coastal salt marsh	Sandy beach	Sand dunes	Savanna	Treeless plains	Water	Wet rainforest				
Predicted type														
Dry rainforest	727	2	17	0	0	2	0	0	0	90	838	0.87	0.13	
Grassland and sedgeland	0	419	14	3	0	5	18	8	0	2	469	0.89	0.11	
Mangrove	55	60	522	0	0	1	0	0	0	69	707	0.74	0.26	
Coastal salt marsh	0	3	1	285	5	1	0	0	2	0	297	0.96	0.04	
Sandy beach	0	0	0	7	356	77	0	0	0	0	440	0.81	0.19	
Sand dunes	0	0	0	2	61	286	0	7	0	0	356	0.80	0.20	
Savanna	2	50	15	0	0	13	754	29	0	20	883	0.85	0.15	
Treeless plains	0	111	3	0	2	145	220	170	0	1	652	0.26	0.74	
Water	0	1	0	3	4	0	0	0	412	0	420	0.98	0.02	
Wet rainforest	358	58	126	0	0	1	31	0	0	251	825	0.30	0.70	
Total	1142	704	698	300	428	531	1023	214	414	433	5887			
PA	0.64	0.60	0.75	0.95	0.83	0.54	0.74	0.79	1.00	0.58				
OE	0.36	0.40	0.25	0.05	0.17	0.46	0.26	0.21	0.00	0.42				

Model formulation

Classification scheme: Ecosystem Functional Group (level 3 of the Global Ecosystem typology)

Satellite/sensor: Sentinel-2/MSI

Covariate set: Satellite image covariates only

PA: Producer's accuracy

UA: User's accuracy

OE: Omission error

CE: Commission error

1042

1043 Table 11. Confusion matrix for the ecosystem functional group classification model using
 1044 Sentinel-2 satellite imagery from the MSI sensor and using satellite image and additional
 1045 covariates.

		Training points										Total	UA	CE
		Dry rainforest	Grassland and sedgeland	Mangrove	Coastal salt marsh	Sandy beach	Sand dunes	Savanna	Treeless plains	Water	Wet rainforest			
Predicted type	Dry rainforest	951	1	11	0	0	1	2	0	0	31	997	0.95	0.05
	Grassland and sedgeland	1	532	28	3	0	20	18	9	0	2	613	0.87	0.13
	Mangrove	57	106	648	0	0	3	1	0	0	7	822	0.79	0.21
	Coastal salt marsh	0	6	1	291	6	4	0	0	0	0	308	0.94	0.06
	Sandy beach	0	0	0	5	391	34	0	0	0	0	430	0.91	0.09
	Sand dunes	0	0	0	1	30	402	2	3	0	0	438	0.92	0.08
	Savanna	1	37	5	0	0	7	900	9	0	21	980	0.92	0.08
	Treeless plains	0	20	0	0	0	60	86	193	0	0	359	0.54	0.46
	Water	0	0	0	0	1	0	0	0	414	0	415	1.00	0.00
	Wet rainforest	132	2	5	0	0	0	14	0	0	372	525	0.71	0.29
	Total	1142	704	698	300	428	531	1023	214	414	433	5887		
PA	0.83	0.76	0.93	0.97	0.91	0.76	0.88	0.90	1.00	0.86				
OE	0.17	0.24	0.07	0.03	0.09	0.24	0.12	0.10	0.00	0.14				

Model formulation

Classification scheme: Ecosystem Functional Group (level 3 of the Global Ecosystem typology)

Satellite/sensor: Sentinel-2/MSI

Covariate set: Satellite image and additional covariates

PA: Producer's accuracy

UA: User's accuracy

OE: Omission error

CE: Commission error

1046

1047 Table 12. Confusion matrix for the biome classification model using Landsat-9 satellite
 1048 imagery from the OLI-2 sensor as the only covariates.

		Training points								Total	UA	CE
		Grassland and sedgeland	Mangrove	Rainforest	Sandy beach	Sand dune	Savanna	Treeless plains	Water			
Predicted type	Grassland and sedgeland	554	48	16	0	3	22	5	0	648	0.85	0.15
	Mangrove	38	867	130	9	0	3	0	2	1049	0.83	0.17
	Rainforest	10	60	1407	0	0	15	0	0	1492	0.94	0.06
	Sandy beach	0	11	0	375	100	0	0	0	486	0.77	0.23
	Sand dunes	1	2	0	42	319	0	4	0	368	0.87	0.13
	Savanna	49	10	22	0	15	848	39	0	983	0.86	0.14
	Treeless plains	51	0	0	0	94	135	166	0	446	0.37	0.63
	Water	1	0	0	2	0	0	0	412	415	0.99	0.01
	Total	704	998	1575	428	531	1023	214	414	5887		
	PA	0.79	0.87	0.89	0.88	0.60	0.83	0.78	1.00			
OE	0.21	0.13	0.11	0.12	0.40	0.17	0.22	0.00				

Model formulation

Classification scheme: Biome (level 2 of the Global Ecosystem typology)

Satellite/sensor: Landsat-9/OLI-2

Covariate set: Satellite image covariates only

PA: Producer's accuracy

UA: User's accuracy

OE: Omission error

CE: Commission error

1049

1050 Table 13. Confusion matrix for the biome classification model using Landsat-9 satellite
 1051 imagery from the OLI-2 sensor and using satellite image and additional covariates.

		Training points								Total	UA	CE
		Grassland and sedgeland	Mangrove	Rainforest	Sandy beach	Sand dune	Savanna	Treeless plains	Water			
Predicted type	Grassland and sedgeland	616	60	17	0	15	14	8	0	730	0.84	0.16
	Mangrove	43	907	31	6	9	1	0	0	997	0.91	0.09
	Rainforest	1	16	1443	0	2	13	0	0	1475	0.98	0.02
	Sandy beach	0	8	0	402	20	0	0	0	430	0.93	0.07
	Sand dunes	0	2	1	19	429	0	0	0	451	0.95	0.05
	Savanna	21	5	83	0	5	911	8	0	1033	0.88	0.12
	Treeless plains	23	0	0	0	51	84	198	0	356	0.56	0.44
	Water	0	0	0	1	0	0	0	414	415	1.00	0.00
	Total	704	998	1575	428	531	1023	214	414	5887		
	PA	0.88	0.91	0.92	0.94	0.81	0.89	0.93	1.00			
OE	0.12	0.09	0.08	0.06	0.19	0.11	0.07	0.00				

Model formulation

Classification scheme: Biome (level 2 of the Global Ecosystem typology)

Satellite/sensor: Landsat-9/OLI-2

Covariate set: Satellite image and additional covariates

PA: Producer's accuracy

UA: User's accuracy

OE: Omission error

CE: Commission error

1052

1053 Table 14. Confusion matrix for the biome classification model using Sentinel-2 satellite
 1054 imagery from the MSI sensor as the only covariates.

		Training points								Total	UA	CE
		Grassland and sedgeland	Mangrove	Rainforest	Sandy beach	Sand dune	Savanna	Treeless plains	Water			
Predicted type	Grassland and sedgeland	449	58	24	0	6	20	9	0	566	0.79	0.21
	Mangrove	64	809	143	4	2	0	0	0	1022	0.79	0.21
	Rainforest	23	92	1358	0	3	5	0	0	1481	0.92	0.08
	Sandy beach	0	8	0	357	74	0	0	4	443	0.81	0.19
	Sand dunes	0	2	0	60	290	0	6	0	358	0.81	0.19
	Savanna	59	22	50	0	14	786	30	0	961	0.82	0.18
	Treeless plains	107	4	0	3	142	212	169	0	637	0.27	0.73
	Water	2	3	0	4	0	0	0	410	419	0.98	0.02
	Total	704	998	1575	428	531	1023	214	414	5887		
	PA	0.64	0.81	0.86	0.83	0.55	0.77	0.79	0.99			
OE	0.36	0.19	0.14	0.17	0.45	0.23	0.21	0.01				

Model formulation

Classification scheme: Biome (level 2 of the Global Ecosystem typology)

Satellite/sensor: Sentinel-2/MSI

Covariate set: Satellite image covariates only

PA: Producer's accuracy

UA: User's accuracy

OE: Omission error

CE: Commission error

1055

1056 Table 15. Confusion matrix for the biome classification model using Sentinel-2 satellite
 1057 imagery from the MSI sensor and using satellite image and additional covariates.

		Training points										
		Grassland and sedgeland	Mangrove	Rainforest	Sandy beach	Sand dune	Savanna	Treeless plains	Water	Total	UA	CE
Predicted type	Grassland and sedgeland	580	80	20	1	32	14	9	0	736	0.79	0.21
	Mangrove	65	880	33	4	19	0	0	0	1001	0.88	0.12
	Rainforest	0	27	1482	0	1	8	0	0	1518	0.98	0.02
	Sandy beach	0	7	0	396	33	0	0	0	436	0.91	0.09
	Sand dunes	1	1	0	26	378	1	1	0	408	0.93	0.07
	Savanna	36	3	40	0	6	911	8	0	1004	0.91	0.09
	Treeless plains	22	0	0	0	62	89	196	0	369	0.53	0.47
	Water	0	0	0	1	0	0	0	414	415	1.00	0.00
	Total	704	998	1575	428	531	1023	214	414	5887		
	PA	0.82	0.88	0.94	0.93	0.71	0.89	0.92	1.00			
OE	0.18	0.12	0.06	0.07	0.29	0.11	0.08	0.00				

Model formulation

Classification scheme: Biome (level 2 of the Global Ecosystem typology)

Satellite/sensor: Sentinel-2/MSI

Covariate set: Satellite image and additional covariates

PA: Producer's accuracy

UA: User's accuracy

OE: Omission error

CE: Commission error

1058 **Additional references**

1059 Aybar, C., Wu, Q., Bautista, L., Yali, R. and Barja, A. (2020) 'rgee: An R package for
 1060 interacting with Google Earth Engine', *Journal of Open Source Software*, 5(51), p. 2272.
 1061 Available at: <https://doi.org/10.21105/joss.02272>.

1062 van den Brand, T. (2024) 'ggh4x: Hacks for "ggplot2"'. Available at: [https://CRAN.R-
 1063 project.org/package=ggh4x](https://CRAN.R-project.org/package=ggh4x).

1064 Campitelli, E. (2023) 'ggnewscale: Multiple Fill and Colour Scales in "ggplot2"'. Available
 1065 at: <https://CRAN.R-project.org/package=ggnewscale>.

1066 Dunnington, D. (2023) 'ggspatial: Spatial Data Framework for ggplot2'. Available at:
 1067 <https://CRAN.R-project.org/package=ggspatial>.

1068 Gorelick, N., Hancher, M., Dixon, M., Ilyushchenko, S., Thau, D. and Moore, R. (2017)
 1069 'Google Earth Engine: Planetary-scale geospatial analysis for everyone', *Remote Sensing of
 1070 Environment*, 202, pp. 18–27. Available at: <https://doi.org/10.1016/j.rse.2017.06.031>.

1071 Greenwell, B.M. and Boehmke, B.C. (2020) 'Variable Importance Plots—An Introduction to
 1072 the vip Package', *The R Journal*, 12(1), pp. 343–366. Available at:
 1073 <https://doi.org/10.32614/RJ-2020-013>.

- 1074 Henry, L., Wickham, H. and Chang, W. (2024) ‘ggstance: Horizontal “ggplot2”
1075 Components’. Available at: <https://CRAN.R-project.org/package=ggstance>.
- 1076 Hernangomez, D. (2024) ‘tidyterra: tidyverse Methods and ggplot2 Helpers for terra
1077 Objects’. Available at: <https://dieghernan.github.io/tidyterra/>.
- 1078 Hijmans, R.J. (2023) ‘terra: Spatial Data Analysis’. Available at: [https://CRAN.R-
1079 project.org/package=terra](https://CRAN.R-project.org/package=terra).
- 1080 Kuhn, M. (2008) ‘Building Predictive Models in R Using the caret Package’, *Journal of
1081 Statistical Software*, 28(5), pp. 1–26. Available at: <https://doi.org/10.18637/jss.v028.i05>.
- 1082 Pebesma, E. (2018) ‘Simple Features for R: Standardized Support for Spatial Vector Data’,
1083 *The R Journal*, 10(1), pp. 439–446. Available at: <https://doi.org/10.32614/RJ-2018-009>.
- 1084 R Core Team (2018) ‘R: A language and environment for statistical computing’. Vienna,
1085 Austria: R Foundation for Statistical Computing.
- 1086 RStudio Team (2020) ‘RStudio: Integrated Development for R’. Boston, MA: RStudio, PBC.
1087 Available at: <http://www.rstudio.com>.
- 1088 Smith, A., Murphy, S., Herderson, D. and Erickson, K. (2023) ‘Including imprecisely
1089 georeferenced specimens improves accuracy of species distribution models and
1090 estimates of niche breadth’, *Global Ecology & Biogeography*, 32(3), pp. 342–355. Available
1091 at: <https://doi.org/doi:10.1111/geb.13628>.
- 1092 Wickham, H. (2016) ‘ggplot2: Elegant Graphics for Data Analysis.’ New York: Springer-
1093 Verlag.
- 1094 Wickham, H. (2022) ‘stringr: Simple, Consistent Wrappers for Common String Operations’.
1095 Available at: <https://CRAN.R-project.org/package=stringr>.
- 1096 Wickham, H., François, R., Harry, L., Müller, K. and Vaughan, D. (2023) ‘dplyr: A Grammar
1097 of Data Manipulation’. Available at: <https://CRAN.R-project.org/package=dplyr>.
- 1098 Wickham, H., Vaughan, D. and Girlich, M. (2023) ‘Tidyr: tidy messy data’. Available at:
1099 <https://CRAN.R-project.org/package=tidyr>.
- 1100 Wright, M.N. and Ziegler, A. (2017) ‘Ranger: a fast implementation of random forests for
1101 high dimensional data in C++ and R.’, *Journal of Statistical Software*, 77(1), pp. 1–17.
1102 Available at: <https://doi.org/doi:10.18637/jss.v077.i01>.
- 1103